

Boundary Criticality of the 3D $O(N)$ Model: From Normal to Extraordinary

Francesco Parisen Toldin*

Institut für Theoretische Physik und Astrophysik, Universität Würzburg, Am Hubland, D-97074 Würzburg, Germany

Max A. Metlitski†

Department of Physics, Massachusetts Institute of Technology, Cambridge, Massachusetts 02139, USA

It was recently realized that the three-dimensional $O(N)$ model possesses an extraordinary boundary universality class for a finite range of $N \geq 2$. For a given N , the existence and universal properties of this class are predicted to be controlled by certain amplitudes of the normal universality class, where one applies an explicit symmetry breaking field to the boundary. In this Letter, we study the normal universality class for $N = 2, 3$ using Monte Carlo simulations on an improved lattice model and extract these universal amplitudes. Our results are in good agreement with direct Monte Carlo studies of the extraordinary universality class serving as a nontrivial quantitative check of the connection between the normal and extraordinary classes.

Introduction.— When a physical system is in the vicinity of a continuous phase transition, various observables develop power-law singularities which have a character of universality: they are determined by the gross features of the system, such as dimensionality and symmetry, and not by the details of local interactions. Renormalization-group (RG) theory allows us to understand the emergence of universality as the result of the existence of fixed points in a suitably defined flow of Hamiltonians. Accordingly, systems exhibiting identical critical behavior define a given universality class (UC) [1]. The presence of a boundary gives rise to rich phenomena, which have attracted a large amount of experimental [2] and theoretical [3–5] studies. General RG arguments show that a given bulk UC class, describing the critical behavior far away from the boundary, potentially admits different surface UCs [1]. Further, surface critical exponents and other universal data generally differ from those of the bulk [3, 4]. Surface UCs also determine the critical Casimir force [6–12]. While boundary criticality is a mature subject, it has recently received renewed attention driven in part by advances in conformal field theory [13–23] and developments in topological phases of quantum matter. Many topological phases including quantum Hall states, topological insulators, and certain quantum spin liquids possess protected boundary states. While it was initially thought that this protection relies on the presence of a bulk energy gap, examples where the boundary state survives in some form even as the bulk gap closes were later discovered [24–32]. The study of such “gapless topological states” and their boundaries lies in the domain of boundary critical phenomena. As gapless topological states were investigated in the context of quantum magnets [33–41], it was realized that even for the simplest model of *classical* magnets—the $O(N)$ model—basic questions about the boundary phase diagram remain open [42–44].

The much investigated classical $O(N)$ model [45] provides a prototypical example of boundary criticality. In three dimensions, for $N = 1, 2$, the bulk-surface phase diagram hosts a surface transition line, where the bulk is disordered and the surface critical behavior belongs to that of 2D $O(N)$ UC. This line terminates at the bulk transition line dividing it into or-

inary and extraordinary surface UCs; the termination point is the so-called special UC [3, 4]. Surprisingly, the surface phase diagram for $N > 2$ is still not fully settled. For $d = 3$ and $N > 2$ there is no surface transition for a disordered bulk [45], thus the topology of the phase diagram does not necessarily dictate the existence of the extraordinary UC or the special multicritical point [46, 47]. Yet, a recent field-theoretical analysis in Ref. [42] has pointed out that if one treats N as a continuous parameter, the extraordinary UC survives for a range $2 < N < N_c$, where N_c is a currently unknown constant. Further, the extraordinary UC in the region $2 \leq N < N_c$ exhibits a surface order parameter correlation function that falls off as

$$\langle \vec{\phi}(\mathbf{x}) \cdot \vec{\phi}(0) \rangle \sim \frac{1}{(\log \mathbf{x})^q}, \quad (1)$$

thus, it was labeled the “extraordinary-log” UC in Ref. [42]; this should be contrasted to the extraordinary transition for $N = 1$ or in $d > 3$ where the above correlation function approaches a constant at large separation. In fact, for $N = 3$ a recent numerical simulation [43] finds firm evidence of a special transition with exponents differing from those of the ordinary UC and a phase consistent with the extraordinary-log UC, implying $N_c > 3$ [48]. For $N = 2$, the “logarithmic” character of the extraordinary phase was also verified numerically [44].

Reference [42] showed that for a given N the existence of the extraordinary-log phase and its properties [such as the exponent q in Eq. (1)] are determined by certain universal amplitudes of the normal boundary UC. The latter is realized when an explicit symmetry breaking field is applied to the boundary [3, 4, 49, 50].

Motivated by these recent developments, in this Letter we study the normal surface UC of the three dimensional $O(N)$ model, for $N = 2$ and $N = 3$, by means of Monte Carlo (MC) simulations of an *improved* lattice model [45], where the leading bulk irrelevant scaling field is suppressed. Through a finite-size scaling analysis of MC data we determine certain universal amplitudes of the normal UC. Such amplitudes are *per se* of interest, as they provide a quantitative description of the normal UC; for $N = 1$ they have been studied in Ref. [51].

Furthermore, exploiting the analysis of Ref. [42], our results confirm the existence of the extraordinary-log UC for $N = 3$, and allow us to compute the universal exponent q in Eq. (1) for $N = 2$ and $N = 3$. Our results are in good agreement with the value of q found in direct studies of the extraordinary phase in Refs. [43, 44].

Model.— We study the classical lattice ϕ^4 model by means of MC simulations. It is defined on a three-dimensional $L_{\parallel} \times L_{\parallel} \times L$ lattice, with periodic boundary conditions (BCs) along the lateral directions with size L_{\parallel} , and open BCs along the remaining direction. The reduced Hamiltonian \mathcal{H} , such that the Gibbs weight is $\exp(-\mathcal{H})$, is

$$\mathcal{H} = -\beta \sum_{\langle i j \rangle} \vec{\phi}_i \cdot \vec{\phi}_j - \beta_s \sum_{\langle i j \rangle_s} \vec{\phi}_i \cdot \vec{\phi}_j - \vec{h}_s \cdot \sum_{i \in s} \vec{\phi}_i + \sum_i [\vec{\phi}_i^2 + \lambda(\vec{\phi}_i^2 - 1)^2], \quad (2)$$

where $\vec{\phi}_x$ is an N -components real field on the lattice site x and the first sum extends over the nearest-neighbor pairs where at least one site belongs to the inner bulk. The second and third sums extend over the lattice sites on the surface. The last term in Eq. (2) is summed over all lattice sites. In Eq. (2) the coupling constant β determines the critical behavior of the bulk, while β_s controls the surface coupling. Finally, we have introduced a symmetry-breaking boundary field $\vec{h}_s = h_s \vec{e}_N$ along the N th direction.

For $\lambda \rightarrow \infty$, the Hamiltonian (2) reduces to the hard spin $O(N)$ model. In the (β, λ) plane, the bulk exhibits a second-order transition line in the $O(N)$ UC [45, 52, 53]. For $N = 2$ the model is *improved* for $\lambda = 2.15(5)$ [53], i.e., the leading bulk irrelevant scaling field with dimension $y_i = -0.789(4)$ [54] is suppressed. At $\lambda = 2.15$ the model is critical for $\beta = 0.50874988(6)$ [55]. For $N = 3$ the model is improved for $\lambda = 5.17(11)$ and the suppressed leading irrelevant scaling field has dimension $y_i = -0.759(2)$ [56]. At $\lambda = 5.2$, the model is critical at $\beta = 0.68798521(8)$ [56]. Improved models are instrumental to obtain accurate results in critical phenomena [45], in particular in boundary critical phenomena [43, 51, 57–65], because the broken translational invariance generically gives rise to additional scaling corrections, which cumulate to those arising from bulk irrelevant operators. The latter are suppressed for improved lattice models, hence enabling a more accurate analysis.

In the MC simulations presented here we set β and λ to the central value of the bulk critical point in the improved models, and $\beta_s = \beta$. Note that the boundary parameters β_s, h_s are chosen to be identical on the two surfaces: this realizes the normal UC on both surfaces, and allows us to compute improved estimators of surface observables by averaging them over the two surfaces. The geometry is fixed by $L = L_{\parallel}$. MC simulations are performed by combining Metropolis, overrelaxation, and Wolff single-cluster updates [66]; details of the algorithm are reported in Ref. [43], and the implementation of the Wolff algorithm in the presence of a symmetry-breaking surface field is discussed in Ref. [51].

The inclusion of a boundary field breaks the $O(N)$ symmetry to $O(N-1)$. Accordingly, we distinguish the components of $\vec{\phi}$ defining $\vec{\phi} \equiv (\vec{\varphi}, \sigma)$, where σ is the component parallel to the surface field, and $\vec{\varphi}$ is a $(N-1)$ -component vector orthogonal to it. As discussed below, we measure the magnetization profile $\langle \sigma \rangle$ and various surface-surface and surface-bulk two-point functions.

Besides the model realizing the normal UC, we also perform some MC simulations of the ϕ^4 model with periodic BCs, with the aim of determining the bulk field normalization. In this case, the Hamiltonian is as in Eq. (2), without the surface terms.

Normal universality class.— In this section, we discuss the normal surface UC of the $O(N)$ model in $d = 3$. Unless otherwise stated, all operators in this section [e.g. $\vec{\phi} = (\vec{\varphi}, \sigma)$] denote continuum fields; when referring to fields of the lattice model (2), we use the subscript “lat”. To leading order, the bulk field $\vec{\phi}_{\text{lat}} \propto \vec{\phi}$. The boundary operator spectrum contains two “protected” operators whose existence is mandated by bulk conservation laws and whose scaling dimensions are known exactly [49, 50, 67]:

- The “tilt” operator t^i of dimension $\hat{\Delta}_t = d - 1 = 2$, which is an $O(N-1)$ vector ($i = 1 \dots N - 1$). This operator is induced on the boundary when the symmetry breaking field \vec{h}_s is tilted—thus the nomenclature [68].
- The displacement operator D of dimension $\hat{\Delta}_D = d = 3$, which is an $O(N-1)$ scalar. Perturbing the boundary with this operator is equivalent to moving the location of the boundary, justifying the name “displacement”.

These are believed to be the two lightest boundary operators. In particular, on the lattice the boundary field $\varphi_{\text{lat}}^i \propto t^i$. The boundary operator product expansion (OPE) holds for $z \rightarrow 0$:

$$\begin{aligned} \sigma(\mathbf{x}, z) &= \frac{a_\sigma}{(2z)^{\Delta_\phi}} + b_D (2z)^{3-\Delta_\phi} D(\mathbf{x}) + \dots, \\ \varphi^i(\mathbf{x}, z) &= b_t (2z)^{2-\Delta_\phi} t^i(\mathbf{x}) + \dots, \end{aligned} \quad (3)$$

where Δ_ϕ is the bulk scaling dimension of $\vec{\phi}$. The coefficients a_σ, b_t, b_D are universal, assuming that the bulk and boundary operators are normalized. a_σ and b_t will be the main target of this Letter—as was shown in Ref. [42], their ratio controls the existence and universal properties of the extraordinary-log phase (in the absence of a boundary magnetic field). Defining

$$\alpha \equiv \frac{\pi}{2} \left(\frac{a_\sigma}{4\pi b_t} \right)^2 - \frac{N-2}{2\pi}, \quad (4)$$

the extraordinary-log phase exists when $\alpha > 0$. Further, the exponent q in Eq. (1) is given by

$$q = \frac{N-1}{2\pi\alpha}. \quad (5)$$

We extract a_σ and b_t from the following correlators, which in a semi-infinite geometry take the form

$$\langle \sigma(z) \rangle = \frac{a_\sigma}{(2z)^{\Delta_\phi}}, \quad \langle t^i(0) \varphi^j(\mathbf{x}, z) \rangle = \delta_{ij} b_t \frac{(2z)^{2-\Delta_\phi}}{(\mathbf{x}^2 + z^2)^2}. \quad (6)$$

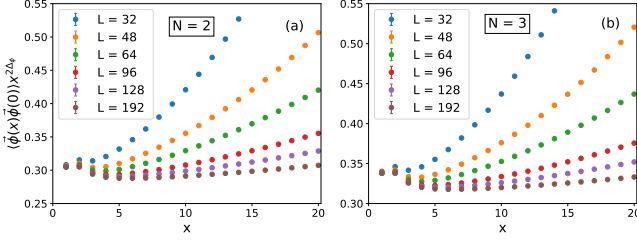


FIG. 1. Bulk two-point function for (a) $N = 2$ and (b) $N = 3$, rescaled to the large-distance decay exponent $2\Delta_\phi$. Error bars are smaller than symbol size.

The bulk field ϕ^a , $a = 1 \dots N$, is normalized so that in an infinite geometry $\langle \phi^a(x) \phi^b(0) \rangle = \delta^{ab} x^{-2\Delta_\phi}$, while t^i is normalized so that in a semi-infinite geometry $\langle t^i(\mathbf{x}) t^j(0) \rangle = \delta^{ij} \mathbf{x}^{-4}$. Thus, in a lattice model, to fix the normalizations above and to find a_σ , b_t we will need to measure four different correlators. On the lattice, we expect both finite size scaling corrections and corrections to scaling [69].

Results.— We study first the XY UC. In order to determine the normalization of the bulk field, we have simulated the ϕ^4 model for $N = 2$, with periodic BCs and at the critical point, for lattice sizes $L = 32 - 192$. In Fig. 1(a) we show the two-point function $\langle \vec{\phi}(x) \cdot \vec{\phi}(0) \rangle$, rescaled to the expected decay $x^{-2\Delta_\phi}$. Here and below we use $\Delta_\phi = 0.519088(22)$, $\Delta_\epsilon = 1.51136(22)$ [70]. We fit the MC data to

$$\langle \vec{\phi}(x) \cdot \vec{\phi}(0) \rangle = \mathcal{N}_{\text{bulk}} x^{-2\Delta_\phi} \left[1 + B_\epsilon \left(\frac{x}{L} \right)^{\Delta_\epsilon} + C x^{-2} \right], \quad (7)$$

where the leading finite-size correction $\propto L^{-\Delta_\epsilon}$ is due to the energy operator in the OPE of $\phi^a \times \phi^a$, while the correction $\propto x^{-2}$ comes from the next-to-leading irrelevant operator in the action and from descendant operators in the expansion of the lattice field $\vec{\phi}_i$ in terms of continuum fields [69]. Equation (7) holds for $(x/L) \ll 1$ and $x \gtrsim x_0$, with x_0 a nonuniversal length governing the two-point function at short distance. The analysis of various fits [71–73] to Eq. (7) allows us to infer [69]:

$$\mathcal{N}_{\text{bulk}} = 0.28152(15), \quad B_\epsilon = 2.758(10). \quad (8)$$

Next, we study the surface critical behavior. As discussed above, in order to implement the normal UC, we simulated the ϕ^4 model at the critical point with open BCs and a symmetry-breaking surface field. Preliminary MC data suggested a reduction of corrections to scaling for a surface field $h_s = 1.5\beta_s$. Our MC simulations reported below have thus been done at this value of h_s , for lattice sizes $L = 32 - 192$. To extract the normalization of the surface field component φ , we have computed its two-point function along the surface. We show it in Fig. 2(a), rescaled to its expected large-distance decay exponent 4. In this case finite-size corrections are rather small, such that we fit the data to [74]

$$\langle \vec{\varphi}(\mathbf{x}) \cdot \vec{\varphi}(0) \rangle = \mathcal{N}_\varphi \mathbf{x}^{-4} (1 + C \mathbf{x}^{-2}), \quad (9)$$

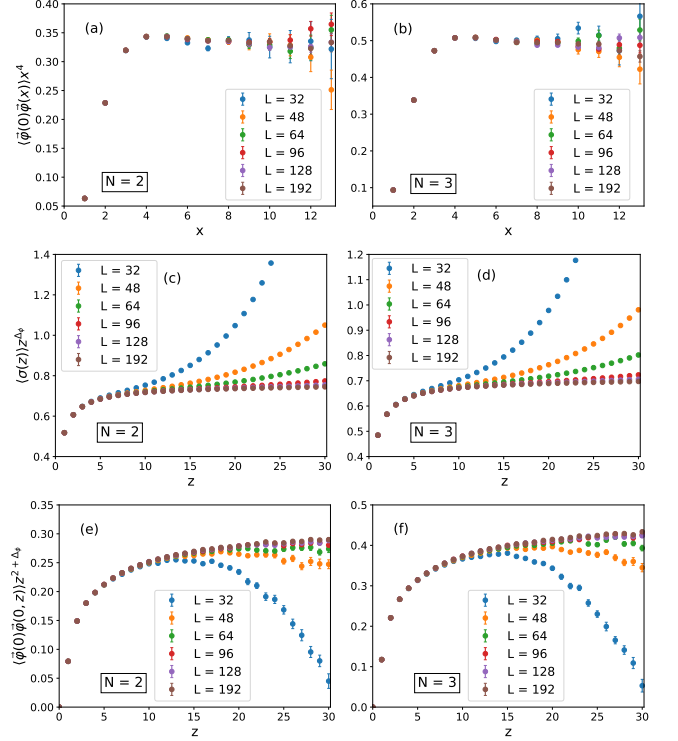


FIG. 2. Plots of surface observables. (a) and (b): Two-point functions of the surface field component φ , for $N = 2$ and $N = 3$, rescaled to the large-distance decay exponent 4. (c) and (d): Order-parameter profile as a function of the distance from the surface, rescaled to the large-distance decay exponent Δ_ϕ . (e) and (f): Surface-bulk correlation functions of the field component φ , rescaled to the large-distance decay exponent $2 + \Delta_\phi$.

where, analogous to Eq. (7), the leading correction to scaling $\propto x^{-2}$ originates from the expansion of the lattice operator in terms of continuum ones. Fits to Eq. (9) deliver [69]

$$\mathcal{N}_\varphi = 0.328(3). \quad (10)$$

In Fig. 2(c), we show the magnetization profile $\langle \sigma(z) \rangle$ as a function of the distance from the surface z , and rescaled to its asymptotic decay exponent Δ_ϕ . For this quantity, scaling and finite-size corrections are relevant and we fit MC data to

$$\langle \sigma(z) \rangle = M_\sigma (z + z_0)^{-\Delta_\phi} \left[1 + B_\sigma \left(\frac{z + z_0}{L} \right)^3 \right], \quad (11)$$

where the perturbation of the surface action with the displacement operator D produces the replacement $z \rightarrow z + z_0$, with z_0 a nonuniversal constant, and the leading finite-size correction originates from the OPE (3) [69]; the latter is also known as distant wall correction [6, 75, 76]. Fits to Eq. (11) allow us to estimate [69]

$$M_\sigma = 0.7540(3), \quad B_\sigma = 1.21(6), \quad z_0 = 1.018(6). \quad (12)$$

In Fig. 2(e) we show the surface-bulk correlation function $\langle \varphi(0) \varphi(0, z) \rangle$ of the field component φ , where one point is

on the surface and the other a distance z away from the surface, so that the vector separating the two points is orthogonal to the surface; the correlations are rescaled to the large-distance decay exponent $2 + \Delta_\phi$. These correlations are affected by significant scaling corrections, while finite-size corrections, though not negligible, are smaller than in the case of $\langle \sigma(z) \rangle$. Together with the relatively fast large-distance decay, $\sim z^{-2-\Delta_\phi}$, this makes the analysis of the surface-bulk correlations more involved. A good ansatz for the MC data is

$$\langle \vec{\varphi}(0) \cdot \vec{\varphi}(0, z) \rangle = M_\varphi (z + z_0)^{-2-\Delta_\phi} \left[1 + B_\varphi \left(\frac{z + z_0}{L} \right)^3 + C(z + z_0)^{-2} \right], \quad (13)$$

where we have included the corrections considered in Eq. (9) and Eq. (11) [69]. To avoid overfitting, in fits to Eq. (13) we plug in the result for z_0 of Eq. (12), varying its value within one error bar quoted there. From the various fits we estimate

$$M_\varphi = 0.3146(8), \quad B_\varphi = -0.7(2). \quad (14)$$

In the analysis of the MC data for the Heisenberg normal UC, we proceed analogous to the case $N = 2$, using the critical exponents $\Delta_\phi = 0.518920(25)$ and $\Delta_\epsilon = 1.5948(2)$ [56]. To extract the normalization of the bulk field ϕ , we simulated the ϕ^4 model for $N = 3$, periodic BCs, and at the critical point, for lattice sizes $L = 32 - 192$. In Fig. 1(b) we show the two-point function of ϕ , rescaled to the expected decay $x^{-2\Delta_\phi}$. From fits of the correlations to Eq. (7) we obtain [69]

$$\mathcal{N}_{\text{bulk}} = 0.31230(15), \quad B_\epsilon = 2.432(7). \quad (15)$$

Concerning the surface critical behavior, preliminary MC simulations of the model (2) with $N = 3$ suggested a reduction of subleading corrections for a surface field $h_s = 1.4\beta_s$. Here, we present results for this choice of h_s , and lattice sizes $L = 32 - 192$. In Fig. 2(b) we show the surface correlations. Fits of $\langle \vec{\varphi}(\mathbf{x}) \cdot \vec{\varphi}(0) \rangle$ to Eq. (9) allow us to estimate [69]

$$\mathcal{N}_\varphi = 0.481(3). \quad (16)$$

Fits of the order-parameter profile $\langle \sigma(z) \rangle$, shown in Fig. 2(d), deliver the following results:

$$M_\sigma = 0.7062(2), \quad B_\sigma = 1.07(5), \quad z_0 = 1.031(4). \quad (17)$$

In Fig. 2(f) we show the surface-bulk correlation function $\langle \vec{\varphi}(0) \cdot \vec{\varphi}(0, z) \rangle$. We fit it to Eq. (13), employing the estimate of z_0 given in Eq. (17). From the various fits we obtain [69]

$$M_\varphi = 0.4674(8), \quad B_\varphi = -0.7(1). \quad (18)$$

Discussion.— According to the discussion above of the normal UC and of the scaling forms in Ref. [69], the results of our scaling analysis of MC data allow us to extract universal amplitudes a_σ, b_t of the normal UC via

$$a_\sigma = \frac{2^{\Delta_\phi} M_\sigma}{\sqrt{\mathcal{N}_{\text{bulk}}/N}}, \quad b_t = \frac{2^{\Delta_\phi} M_\varphi}{4\sqrt{N-1}\sqrt{\mathcal{N}_{\text{bulk}}/N}\sqrt{\mathcal{N}_\varphi}}. \quad (19)$$

N	a_σ	b_t	b_D	α	α_{eo}
1	2.60(5)		0.244(8)		
2	2.880(2)	0.525(4)		0.300(5)	0.27(2)[44]
3	3.136(2)	0.529(3)		0.190(4)	0.15(2)[43]

TABLE I. Final results: universal amplitudes a_σ, b_t, b_D in Eq. (3) together with the corresponding value of α , Eq. (4). We also tabulate α_{eo} found in Refs. [43, 44] by direct MC simulations of the extraordinary region. For $N = 1$ we present the values of a_σ, b_D extracted from MC results of Refs. [51, 58].

a_σ is obtained from the amplitude of the order-parameter profile M_σ (11) and the normalization of the bulk field $\mathcal{N}_{\text{bulk}}$ (7), while b_t is obtained in terms of the amplitude of the surface-bulk correlations M_φ (13), and the bulk and surface normalizations $\mathcal{N}_{\text{bulk}}$, (7), \mathcal{N}_φ , (9). We collect our results for a_σ, b_t in Table I, including the value of α obtained from a_σ and b_t via Eq. (4). For both $N = 2$ and $N = 3$, $\alpha > 0$, which indicates that the extraordinary-log UC exists, in accord with MC results of Refs. [43, 44]. Reference [42] predicts that α controls various universal properties of the extraordinary-log phase, including the exponent q in Eq. (1), which is related to α via Eq. (5). α found here agrees well with α extracted from direct MC simulations of the extraordinary region [43, 44], listed in Table I as α_{eo} . This provides a highly nontrivial check of the theory in Ref. [42]. As pointed out in Ref. [43], the error bar on α_{eo} should be taken with a grain of salt given the difficulty of fitting to the form in Eq. (1) and the presence of subleading logarithmic corrections. Thus, we expect the method for determining α presented here to be more reliable than directly simulating the extraordinary-log phase. We also present results for the coefficients a_σ, b_D in Eq. (3) for the normal UC of the Ising model ($N = 1$) [69, 77–84], extracted from MC studies in Refs. [51, 58]. A numerical conformal bootstrap study of the normal UC of the $O(N)$ model with $N \geq 2$ was conducted in parallel to our work [68]. Our results for a_σ and b_t are within the bounds produced by positive bootstrap and agree reasonably well with the approximate truncated bootstrap results. For $N = 1$, both a_σ and b_D in Table I agree within error bars with the truncated bootstrap findings of Ref. [85].

We conclude by outlining some possible future directions. It will be interesting to extend the calculations presented here to the $O(N)$ model with $N > 3$, with an eye to determining the critical value N_c where the extraordinary-log UC disappears. $N = 4$ is a natural first target since bootstrap calculations [68], as well as previous MC simulations [86], suggest that the extraordinary transition still exists in this case. Another extension is to study the free energy density for the normal UC in the geometry considered here, which combined with the coefficient B_σ in Eq. (11) and a_σ , allows one to determine the OPE coefficient b_D in Eq. (3), as well as the universal coefficient C_D , characterizing the boundary OPE of the energy-momentum tensor $T_{zz} \xrightarrow{z \rightarrow 0} -\sqrt{C_D}D$ [67]. (In fact, this is how for the Ising model b_D in Table I was obtained

[87].) Further interesting avenues for future research would be to consider the $N \rightarrow 0$ limit [88–93], which describes the physics of dilute polymers [1, 45, 94], and $O(N)$ loop models [95, 96], which provide an extension of the standard $O(N)$ model to noninteger values of N .

We are very grateful to Marco Meineri for discussions. M.M. thanks Ilya Gruzberg, Abijith Krishnan, Marco Meineri and Jay Padaysi for a collaboration on a related project. We thank Jian-Ping Lv for useful communications. F.P.T. is funded by the Deutsche Forschungsgemeinschaft (DFG, German Research Foundation)—Project No. 414456783. We gratefully acknowledge the Gauss Centre for Supercomputing e.V. for funding this project by providing computing time through the John von Neumann Institute for Computing (NIC) on the GCS Supercomputer JUWELS at Jülich Supercomputing Centre (JSC) [97]. M.M. is supported by the National Science Foundation under Grant No. DMR-1847861.

* francesco.parisentoldin@physik.uni-wuerzburg.de

† mmetlits@mit.edu

- [1] J. Cardy, *Scaling and Renormalization in Statistical Physics* (Cambridge University Press, Cambridge, 1996).
- [2] H. Dosch, *Critical Phenomena at Surfaces and Interfaces: Evanescent X-Ray and Neutron Scattering*, Springer Tracts in Modern Physics (Springer Berlin Heidelberg, Berlin, 2006).
- [3] K. Binder, Critical behavior at surfaces, in *Phase Transitions and Critical Phenomena*, Vol. 8, edited by C. Domb and J. L. Lebowitz (Academic Press, London, 1983) p. 1.
- [4] H. W. Diehl, Field-theoretical approach to critical behaviour at surfaces, in *Phase Transitions and Critical Phenomena*, Vol. 10, edited by C. Domb and J. L. Lebowitz (Academic Press, London, 1986) p. 75.
- [5] M. Pleimling, Critical phenomena at perfect and non-perfect surfaces, *J. Phys. A: Math. Gen.* **37**, R79 (2004), [cond-mat/0402574](#).
- [6] M. E. Fisher and P.-G. de Gennes, Phénomènes aux parois dans un mélange binaire critique, *C. R. Acad. Sci. Paris Ser. B* **287**, 207 (1978).
- [7] M. Krech, *The Casimir Effect in Critical Systems* (World Scientific, London, 1994).
- [8] M. Krech, Fluctuation-induced forces in critical fluids, *J. Phys.: Condens. Matter* **11**, R391 (1999), [cond-mat/9909413](#).
- [9] Ī. Brankov, D. Danchev, and N. Tonchev, *Theory of Critical Phenomena in Finite-size Systems: Scaling and Quantum Effects*, Series in modern condensed matter physics (World Scientific, Singapore, 2000).
- [10] A. Gambassi, The Casimir effect: From quantum to critical fluctuations, *J. Phys.: Conf. Ser.* **161**, 012037 (2009), [arXiv:0812.0935 \[cond-mat.stat-mech\]](#).
- [11] A. Gambassi and S. Dietrich, Critical Casimir forces steered by patterned substrates, *Soft Matter* **7**, 1247 (2011), [arXiv:1011.1831 \[cond-mat.soft\]](#).
- [12] A. Maciołek and S. Dietrich, Collective behavior of colloids due to critical Casimir interactions, *Rev. Mod. Phys.* **90**, 045001 (2018), [arXiv:1712.06678 \[cond-mat.soft\]](#).
- [13] D. McAvity and H. Osborn, Conformal field theories near a boundary in general dimensions, *Nucl. Phys.* **B455**, 522 (1995), [arXiv:cond-mat/9505127 \[cond-mat\]](#).
- [14] P. Liendo, L. Rastelli, and B. C. van Rees, The bootstrap program for boundary CFT_d, *JHEP* **07** (2013), 113, [arXiv:1210.4258 \[hep-th\]](#).
- [15] F. Gliozzi, P. Liendo, M. Meineri, and A. Rago, Boundary and Interface CFTs from the Conformal Bootstrap, *JHEP* **05** (2015), 036, [arXiv:1502.07217 \[hep-th\]](#).
- [16] M. Billó, V. Gonçalves, E. Lauria, and M. Meineri, Defects in conformal field theory, *JHEP* **04** (2016), 091, [arXiv:1601.02883 \[hep-th\]](#).
- [17] P. Liendo and C. Meneghelli, Bootstrap equations for $\mathcal{N} = 4$ SYM with defects, *JHEP* **01** (2017), 122, [arXiv:1608.05126 \[hep-th\]](#).
- [18] E. Lauria, M. Meineri, and E. Trevisani, Radial coordinates for defect CFTs, *JHEP* **11** (2018), 148, [arXiv:1712.07668 \[hep-th\]](#).
- [19] D. Mazáč, L. Rastelli, and X. Zhou, An analytic approach to BCFT_d, *JHEP* **12** (2019), 004, [arXiv:1812.09314 \[hep-th\]](#).
- [20] A. Kaviraj and M. F. Paulos, The functional bootstrap for boundary CFT, *JHEP* **04** (2020), 135, [arXiv:1812.04034 \[hep-th\]](#).
- [21] P. Dey, T. Hansen, and M. Shpot, Operator expansions, layer susceptibility and two-point functions in BCFT, *JHEP* **12** (2020), 051, [arXiv:2006.11253 \[hep-th\]](#).
- [22] C. Behan, L. Di Pietro, E. Lauria, and B. C. Van Rees, Bootstrapping boundary-localized interactions, *JHEP* **12** (2020), 182, [arXiv:2009.03336 \[hep-th\]](#).
- [23] A. Gimenez-Grau, P. Liendo, and P. van Vliet, Superconformal boundaries in $4 - \epsilon$ dimensions, *JHEP* **04** (2021), 167, [arXiv:2012.00018 \[hep-th\]](#).
- [24] T. Grover and A. Vishwanath, Quantum criticality in topological insulators and superconductors: Emergence of strongly coupled majoranas and supersymmetry, [arXiv:1206.1332 \[cond-mat.str-el\]](#).
- [25] M. Barkeshli, M. Mulligan, and M. P. A. Fisher, Particle-hole symmetry and the composite fermi liquid, *Phys. Rev. B* **92**, 165125 (2015), [arXiv:1502.05404 \[cond-mat.str-el\]](#).
- [26] M. Barkeshli and X.-L. Qi, Synthetic topological qubits in conventional bilayer quantum hall systems, *Phys. Rev. X* **4**, 041035 (2014), [arXiv:1302.2673 \[cond-mat.mes-hall\]](#).
- [27] J. Cano, M. Cheng, M. Barkeshli, D. J. Clarke, and C. Nayak, Chirality-protected majorana zero modes at the gapless edge of abelian quantum hall states, *Phys. Rev. B* **92**, 195152 (2015), [arXiv:1505.07825 \[cond-mat.str-el\]](#).
- [28] T. Scaffidi, D. E. Parker, and R. Vasseur, Gapless symmetry-protected topological order, *Phys. Rev. X* **7**, 041048 (2017), [arXiv:1705.01557 \[cond-mat.str-el\]](#).
- [29] D. E. Parker, T. Scaffidi, and R. Vasseur, Topological luttinger liquids from decorated domain walls, *Phys. Rev. B* **97**, 165114 (2018), [arXiv:1711.09106 \[cond-mat.str-el\]](#).
- [30] R. Verresen, R. Thorngren, N. G. Jones, and F. Pollmann, Gapless topological phases and symmetry-enriched quantum criticality, *Phys. Rev. X* **11**, 041059 (2021), [arXiv:1905.06969 \[cond-mat.str-el\]](#).
- [31] R. Verresen, Topology and edge states survive quantum criticality between topological insulators, [arXiv:2003.05453 \[cond-mat.str-el\]](#).
- [32] R. Thorngren, A. Vishwanath, and R. Verresen, Intrinsically gapless topological phases, *Phys. Rev. B* **104**, 075132 (2021), [arXiv:2008.06638 \[cond-mat.str-el\]](#).
- [33] T. Suzuki and M. Sato, Gapless edge states and their stability in two-dimensional quantum magnets, *Phys. Rev. B* **86**, 224411 (2012), [arXiv:1209.3097 \[cond-mat.str-el\]](#).
- [34] L. Zhang and F. Wang, Unconventional Surface Critical Behavior Induced by a Quantum Phase Transition from the Two-Dimensional Affleck-Kennedy-Lieb-Tasaki Phase to a

- Néel-Ordered Phase, *Phys. Rev. Lett.* **118**, 087201 (2017), arXiv:1611.06477 [cond-mat.str-el].
- [35] C. Ding, L. Zhang, and W. Guo, Engineering Surface Critical Behavior of (2+1)-Dimensional O(3) Quantum Critical Points, *Phys. Rev. Lett.* **120**, 235701 (2018), arXiv:1801.10035 [cond-mat.str-el].
- [36] L. Weber, F. Parisen Toldin, and S. Wessel, Nonordinary edge criticality of two-dimensional quantum critical magnets, *Phys. Rev. B* **98**, 140403(R) (2018), arXiv:1804.06820 [cond-mat.str-el].
- [37] L. Weber and S. Wessel, Nonordinary criticality at the edges of planar spin-1 heisenberg antiferromagnets, *Phys. Rev. B* **100**, 054437 (2019), arXiv:1906.07051 [cond-mat.str-el].
- [38] C.-M. Jian, Y. Xu, X.-C. Wu, and C. Xu, Continuous Néel-VBS quantum phase transition in non-local one-dimensional systems with SO(3) symmetry, *SciPost Phys.* **10**, 033 (2021), arXiv:2004.07852 [cond-mat.str-el].
- [39] W. Zhu, C. Ding, L. Zhang, and W. Guo, Surface critical behavior of coupled Haldane chains, *Phys. Rev. B* **103**, 024412 (2021), arXiv:2010.10920 [cond-mat.str-el].
- [40] L. Weber and S. Wessel, Spin versus bond correlations along dangling edges of quantum critical magnets, *Phys. Rev. B* **103**, L020406 (2021), arXiv:2010.15691 [cond-mat.str-el].
- [41] C. Ding, W. Zhu, W. Guo, and L. Zhang, Special Transition and Extraordinary Phase on the Surface of a (2+1)-Dimensional Quantum Heisenberg Antiferromagnet, , arXiv:2110.04762 (2021), arXiv:2110.04762 [cond-mat.str-el].
- [42] M. A. Metlitski, Boundary criticality of the O(N) model in $d = 3$ critically revisited, *Scipost* **12**, 131 (2022), arXiv:2009.05119 [cond-mat.str-el].
- [43] F. Parisen Toldin, Boundary critical behavior of the three-dimensional Heisenberg universality class, *Phys. Rev. Lett.* **126**, 135701 (2021), arXiv:2012.00039 [cond-mat.stat-mech].
- [44] M. Hu, Y. Deng, and J.-P. Lv, Extraordinary-Log Surface Phase Transition in the Three-Dimensional X Y Model, *Phys. Rev. Lett.* **127**, 120603 (2021), arXiv:2104.05152 [cond-mat.stat-mech].
- [45] A. Pelissetto and E. Vicari, Critical phenomena and renormalization-group theory, *Phys. Rep.* **368**, 549 (2002), cond-mat/0012164.
- [46] M. Krech, Surface scaling behavior of isotropic heisenberg systems: Critical exponents, structure factor, and profiles, *Phys. Rev. B* **62**, 6360 (2000), arXiv:cond-mat/0006448 [cond-mat.stat-mech].
- [47] Y. Deng, H. W. J. Blöte, and M. P. Nightingale, Surface and bulk transitions in three-dimensional O(n) models, *Phys. Rev. E* **72**, 016128 (2005), cond-mat/0504173 [cond-mat.stat-mech].
- [48] Earlier a hint of the special transition for $N = 3$ was seen in Ref. [47].
- [49] A. J. Bray and M. A. Moore, Critical behaviour of semi-infinite systems, *J. Phys. A: Math. Gen.* **10**, 1927 (1977).
- [50] T. W. Burkhardt and J. L. Cardy, Surface critical behaviour and local operators with boundary-induced critical profiles, *J. Phys. A: Math. Gen.* **20**, L233 (1987).
- [51] F. Parisen Toldin and S. Dietrich, Critical Casimir forces and adsorption profiles in the presence of a chemically structured substrate, *JSTAT* (2010), P11003, arXiv:1007.3913 [cond-mat.stat-mech].
- [52] M. Campostrini, M. Hasenbusch, A. Pelissetto, P. Rossi, and E. Vicari, Critical exponents and equation of state of the three-dimensional Heisenberg universality class, *Phys. Rev. B* **65**, 144520 (2002), cond-mat/0110336.
- [53] M. Campostrini, M. Hasenbusch, A. Pelissetto, and E. Vicari, Theoretical estimates of the critical exponents of the superfluid transition in ^4He by lattice methods, *Phys. Rev. B* **74**, 144506 (2006), cond-mat/0605083.
- [54] M. Hasenbusch, Monte Carlo study of an improved clock model in three dimensions, *Phys. Rev. B* **100**, 224517 (2019), arXiv:1910.05916 [cond-mat.stat-mech].
- [55] F. Parisen Toldin, Finite-Size Scaling at fixed Renormalization-Group invariant, *Phys. Rev. E* **105**, 034137 (2022), arXiv:2112.00392 [cond-mat.stat-mech].
- [56] M. Hasenbusch, Monte carlo study of a generalized icosahedral model on the simple cubic lattice, *Phys. Rev. B* **102**, 024406 (2020), arXiv:2005.04448 [cond-mat.stat-mech].
- [57] M. Hasenbusch, The thermodynamic Casimir effect in the neighbourhood of the λ -transition: a Monte Carlo study of an improved three-dimensional lattice model, *JSTAT* (2010), P07031, arXiv:0905.2096 [cond-mat.stat-mech].
- [58] M. Hasenbusch, Thermodynamic Casimir effect for films in the three-dimensional Ising universality class: Symmetry-breaking boundary conditions, *Phys. Rev. B* **82**, 104425 (2010), arXiv:1005.4749 [cond-mat.stat-mech].
- [59] M. Hasenbusch, Thermodynamic Casimir force: A Monte Carlo study of the crossover between the ordinary and the normal surface universality class, *Phys. Rev. B* **83**, 134425 (2011), arXiv:1012.4986 [cond-mat.stat-mech].
- [60] M. Hasenbusch, Monte Carlo study of surface critical phenomena: The special point, *Phys. Rev. B* **84**, 134405 (2011), arXiv:1108.2425 [cond-mat.stat-mech].
- [61] M. Hasenbusch, Thermodynamic Casimir effect: Universality and corrections to scaling, *Phys. Rev. B* **85**, 174421 (2012), arXiv:1202.6206 [cond-mat.stat-mech].
- [62] F. Parisen Toldin, M. Tröndle, and S. Dietrich, Critical Casimir forces between homogeneous and chemically striped surfaces, *Phys. Rev. E* **88**, 052110 (2013), arXiv:1303.6104 [cond-mat.stat-mech].
- [63] F. Parisen Toldin, Critical Casimir force in the presence of random local adsorption preference, *Phys. Rev. E* **91**, 032105 (2015), arXiv:1308.5220 [cond-mat.stat-mech].
- [64] F. Parisen Toldin, M. Tröndle, and S. Dietrich, Line contribution to the critical Casimir force between a homogeneous and a chemically stepped surface, *J. Phys.: Condens. Matter* **27**, 214010 (2015), arXiv:1409.5536 [cond-mat.stat-mech].
- [65] F. Parisen Toldin, F. F. Assaad, and S. Wessel, Critical behavior in the presence of an order-parameter pinning field, *Phys. Rev. B* **95**, 014401 (2017), arXiv:1607.04270 [cond-mat.stat-mech].
- [66] U. Wolff, Collective Monte Carlo updating for spin systems, *Phys. Rev. Lett.* **62**, 361 (1989).
- [67] J. L. Cardy, Universal critical-point amplitudes in parallel-plate geometries, *Phys. Rev. Lett.* **65**, 1443 (1990).
- [68] J. Padayasi, A. Krishnan, M. Metlitski, I. Gruzberg, and M. Meineri, The extraordinary boundary transition in the 3d o(n) model via conformal bootstrap, arXiv:2111.03071 [cond-mat.str-el].
- [69] See Supplemental Material for a discussion of the scaling forms of various observables of the lattice model, technical details on the fits of statistically correlated data, and results of the fits of MC data.
- [70] S. M. Chester, W. Landry, J. Liu, D. Poland, D. Simmons-Duffin, N. Su, and A. Vichi, Carving out OPE space and precise O(2) model critical exponents, *JHEP* **06** (2020), 142, arXiv:1912.03324 [hep-th].
- [71] A. P. Young, *Everything You Wanted to Know About Data Analysis and Fitting but Were Afraid to Ask*, Springer-Briefs in Physics (Springer International Publishing, 2015) arXiv:1210.3781.
- [72] C. Michael, Fitting correlated data, *Phys. Rev. D* **49**, 2616

- (1994), arXiv:hep-lat/9310026 [hep-lat].
- [73] D. Seibert, Undesirable effects of covariance matrix techniques for error analysis, *Phys. Rev. D* **49**, 6240 (1994), arXiv:hep-lat/9305014 [hep-lat].
- [74] Even though $\vec{\varphi}$ has only a single component in the $N = 2$ case, we write it as a vector here to set the normalization for $N = 3$.
- [75] E. Eisenriegler, M. Krech, and S. Dietrich, Absence of hyperuniversality in critical films, *Phys. Rev. Lett.* **70**, 619 (1993); Erratum: “Absence of hyperuniversality in critical films” [*Phys. Rev. Lett.* **70**, 619 (1993)], *Phys. Rev. Lett.* **70**, 2051(E) (1993).
- [76] E. Eisenriegler and M. Stapper, Critical behavior near a symmetry-breaking surface and the stress tensor, *Phys. Rev. B* **50**, 10009 (1994).
- [77] D. Simmons-Duffin, The Lightcone Bootstrap and the Spectrum of the 3d Ising CFT, *JHEP* **03** (2017), 086, arXiv:1612.08471 [hep-th].
- [78] M. Hasenbusch, Universal amplitude ratios in the three-dimensional Ising universality class, *Phys. Rev. B* **82**, 174434 (2010), arXiv:1004.4983 [cond-mat.stat-mech].
- [79] M. Campostrini, A. Pelissetto, P. Rossi, and E. Vicari, 25th-order high-temperature expansion results for three-dimensional Ising-like systems on the simple-cubic lattice, *Phys. Rev. E* **65**, 066127 (2002), cond-mat/0201180.
- [80] A. J. Bray, Dispersion-theory approach to the correlation function for critical scattering, *Phys. Rev. B* **14**, 1248 (1976).
- [81] R. F. Chang, H. Burstyn, and J. V. Sengers, Correlation function near the critical mixing point of a binary liquid, *Phys. Rev. A* **19**, 866 (1979).
- [82] P. Damay, F. Leclercq, and P. Chieux, Critical scattering function in a binary fluid mixture: A study of sodium-deuteroammonia solution at the critical concentration by small-angle neutron scattering, *Phys. Rev. B* **40**, 4696 (1989).
- [83] P. Damay, F. Leclercq, R. Magli, F. Formisano, and P. Lindner, Universal critical-scattering function: An experimental approach, *Phys. Rev. B* **58**, 12038 (1998).
- [84] V. Martín-Mayor, A. Pelissetto, and E. Vicari, Critical structure factor in ising systems, *Phys. Rev. E* **66**, 026112 (2002).
- [85] F. Gliozzi, P. Liendo, M. Meineri, and A. Rago, Boundary and interface CFTs from the conformal bootstrap, *JHEP* **05** (2015), 036, arXiv:1502.07217 [hep-th].
- [86] Y. Deng, Bulk and surface phase transitions in the three-dimensional $O(4)$ spin model, *Phys. Rev. E* **73**, 056116 (2006).
- [87] In principle, it is also possible to determine b_D by a method similar to the one we used to find b_t : one extracts the normalization of D from the connected two-point function of σ on the boundary, and the coefficient b_D from the connected bulk-boundary two point function of σ . However, we found that due to the large scaling dimension $\hat{\Delta}_D = 3$, the boundary two-point function $\langle \sigma(\mathbf{x})\sigma(0) \rangle_{\text{conn}}$ falls off very fast, so that the normalization is difficult to extract reliably.
- [88] K. De’Bell, T. Lookman, and S. G. Whittington, Analysis of exact enumeration data for self-avoiding walks attached to a surface, *Phys. Rev. A* **41**, 682 (1990).
- [89] K. De’Bell and T. Lookman, Surface phase transitions in polymer systems, *Rev. Mod. Phys.* **65**, 87 (1993).
- [90] D. Zhao, T. Lookman, and K. De’Bell, Crossover behavior for self-avoiding walks interacting with a surface, *Phys. Rev. A* **42**, 4591 (1990).
- [91] E. Eisenriegler, *Polymers Near Surfaces* (World Scientific, Singapore, 1993).
- [92] R. Hegger and P. Grassberger, Chain polymers near an adsorbing surface, *J. Phys. A: Math. Gen.* **27**, 4069 (1994).
- [93] M. T. Batchelor and J. Cardy, Extraordinary transition in the two-dimensional $o(n)$ model, *Nucl. Phys. B* **506**, 553–564 (1997).
- [94] P.-G. de Gennes, *Scaling Concepts in Polymer Physics* (Cornell University Press, Ithaca, NY, 1979).
- [95] Q. Liu, Y. Deng, T. M. Garoni, and H. W. J. Blöte, The $O(n)$ loop model on a three-dimensional lattice, *Nucl. Phys. B* **859**, 107 (2012), arXiv:1112.5647 [cond-mat.stat-mech].
- [96] E. Domany, D. Mukamel, B. Nienhuis, and A. Schwimmer, Duality relations and equivalences for models with $O(N)$ and cubic symmetry, *Nucl. Phys. B* **190**, 279 (1981).
- [97] Jülich Supercomputing Centre, JUWELS: Modular Tier-0/1 Supercomputer at the Jülich Supercomputing Centre, *J. Large-Scale Res. Facil.* **5**, A135 (2019).

Supplemental Material

SCALING FORMS

In this section, we discuss the scaling forms of various observables for the normal boundary universality class of the $O(N)$ model that we use to fit our data. We always assume that the model is tuned to the bulk critical point. Unless otherwise noted, all the operators in this section are those of the continuum conformal field theory; lattice fields are denoted with an explicit subscript “lat”. We will denote bulk operators by \mathcal{O} and boundary operators (with the exception of protected operators) by $\hat{\mathcal{O}}$ and the corresponding scaling dimensions by $\Delta_{\mathcal{O}}$ and $\hat{\Delta}_{\mathcal{O}}$. We normalize bulk operators so that in infinite space $\langle \mathcal{O}_1(x)\mathcal{O}_2(y) \rangle = \frac{\delta_{12}}{(x-y)^{2\Delta_{\mathcal{O}}}}$, and boundary operators so that in half-infinite space $\langle \hat{\mathcal{O}}_1(\mathbf{x})\hat{\mathcal{O}}_2(\mathbf{y}) \rangle = \frac{\delta_{12}}{(\mathbf{x}-\mathbf{y})^{2\Delta_{\mathcal{O}}}}$.

We begin with the bulk OPE of the leading $O(N)$ vector ϕ^a with itself: $\phi^a \times \phi^b$. This OPE will contain operators transforming in the singlet, traceless symmetric and antisymmetric tensor representations of $O(N)$. After taking the $O(N)$ trace, only the $O(N)$ singlet operators survive:

$$\phi^a(x)\phi^a(0) = \frac{N}{x^{2\Delta_{\phi}}} (1 + \lambda_{\phi\phi\epsilon} x^{\Delta_{\epsilon}} \epsilon(0) + \dots), \quad x \rightarrow 0. \quad (\text{S.1})$$

Here, ϵ is the lowest dimension singlet — the relevant perturbation of the $O(N)$ model, often called the thermal or the energy operator, and $\lambda_{\phi\phi\epsilon}$ is an OPE coefficient. We have dropped all higher dimension operators in the OPE. When considering the system in a periodic box of size L , we expect $\langle \epsilon(x) \rangle = \frac{u_{\epsilon}}{L^{\Delta_{\epsilon}}}$, with u_{ϵ} — a universal number. Thus, in a periodic box the two point function including the leading finite size scaling correction is:

$$\langle \phi^a(x)\phi^a(0) \rangle \approx \frac{N}{x^{2\Delta_{\phi}}} \left[1 + \lambda_{\phi\phi\epsilon} u_{\epsilon} \left(\frac{x}{L} \right)^{\Delta_{\epsilon}} \right], \quad x \ll L. \quad (\text{S.2})$$

We also expect corrections to scaling. We are working with a model where the leading irrelevant $O(N)$ scalar ϵ' has been tuned away. Thus, corrections to scaling will come from a variety of sources:

1. The next $O(N)$ scalar and angular momentum $\ell = 0$ perturbation ϵ'' — the dimension of this is not known precisely for $N \geq 2$. For $N = 1$ numerical bootstrap gives $\Delta_{\epsilon''} \approx 6.9$ [77], i.e. the correction to scaling exponent $\omega'' \approx 3.9$. These corrections will be ignored below.
2. The leading $O(N)$ scalar and angular momentum $\ell = 4$ perturbation (which is allowed by the cubic anisotropy of the lattice) - this is estimated to have scaling dimension $\Delta \approx 5$, so $\omega_{NR} \approx 2$ [54, 56, 77].
3. The expansion of the lattice operator in terms of continuum operators,

$$\phi_{\text{lat}}^a \approx \sqrt{\mathcal{N}_{\text{bulk}}/N} (1 + c \square) \phi^a + \dots, \quad (\text{S.3})$$

where we’ve dropped higher descendants of ϕ^a , as well as higher dimension $O(N)$ vector primaries (it is generally thought that they have dimension $\Delta > 3 > \Delta_{\phi} + 2$).

Combining the effects 2 and 3 we obtain our scaling ansatz (7). Note that we have only included corrections to scaling to the leading term in the $x \ll L$ limit in (7).

We next proceed to the theory in the presence of a normal boundary. We begin by taking the expectation value of the σ OPE in (3). In a periodic slab geometry, $\langle D \rangle = u_D L^{-3}$, so we obtain

$$\langle \sigma(z) \rangle \approx \frac{a_{\sigma}}{(2z)^{\Delta_{\phi}}} \left[1 + \frac{8b_D u_D}{a_{\sigma}} \left(\frac{z}{L} \right)^3 \right], \quad z \ll L. \quad (\text{S.4})$$

What are the corrections to scaling to the above form? The corrections 2 and 3 discussed for the bulk correlator are still present. In addition, there are corrections due to irrelevant perturbations on the boundary: the lowest of these is the displacement D , whose effect is to replace $z \rightarrow z + z_0$ in Eq. (S.4). Here z_0 is a non-universal constant with units of length. Indeed, we have the boundary OPE, $T^{zz} \sim -\sqrt{C_D} D$, $z \rightarrow 0$, where $T^{\mu\nu}$ is the stress-tensor and C_D - a universal constant. Thus, perturbing the boundary with the displacement changes the action by $\delta S = z_0 \int d^2\mathbf{x} (T^{zz}(z=0, \mathbf{x}) + T^{zz}(z=L, \mathbf{x}))$, where we’ve assumed reflection symmetry $z \rightarrow L - z$. Then

$$\langle \sigma(z) \rangle_{S+\delta S} = \langle \sigma(z+z_0) \rangle_{S+\delta S'} \quad (\text{S.5})$$

with $\delta S' = 2z_0 \int d^2\mathbf{x} T^{zz}(z=L, \mathbf{x})$. Here, we’ve moved one insertion of the stress-tensor from $z=0$ to $z=L$. With the perturbation $\delta S'$ localized on the $z=L$ boundary, for $z \ll L$ we can now use the OPE (3) on the right-hand-side of (S.5). We will have $\langle D \rangle_{S+\delta S'} = u_D L^{-3} (1 + O(1/L))$. Thus, including $1/z$ corrections to the second term in brackets in Eq. (S.4), but not $1/L$ corrections (which are smaller in the $z \ll L$ limit), we obtain Eq. (S.4) with $z \rightarrow z + z_0$. We will ignore corrections to scaling from irrelevant boundary operators above D : according to large- N analysis, the lowest of these has $\hat{\Delta} = 5$ [68], which will lead to $\omega = 3$. Thus, we obtain the ansatz

$$\langle \sigma_{\text{lat}}(z) \rangle \approx M_{\sigma}(z+z_0)^{-\Delta_{\phi}} \left[1 + B_{\sigma} \left(\frac{z+z_0}{L} \right)^3 + C(z+z_0)^{-2} \right] \quad (\text{S.6})$$

with

$$M_{\sigma} = 2^{-\Delta_{\phi}} a_{\sigma} \sqrt{\mathcal{N}_{\text{bulk}}/N}. \quad (\text{S.7})$$

Note that the replacement $z \rightarrow z + z_0$ in the C term is for esthetic purposes — we do not claim to know the corrections to such accuracy.

We next discuss the boundary two-point function $\langle \varphi_{\text{lat}}^i(\mathbf{x}) \varphi_{\text{lat}}^i(0) \rangle$. The leading contribution to the boundary lattice field is from the tilt operator t^i :

$$\varphi_{\text{lat}}^i(\mathbf{x}) = \sqrt{\mathcal{N}_\varphi / (N-1)} (1 + c \square_{\mathbf{x}}) t^i(\mathbf{x}) + \dots \quad (\text{S.8})$$

We neglect higher dimension boundary primaries in the above expansion: in the large- N limit these start with $\hat{\Delta} = 5$ [68]. Now, we have the OPE

$$t^i(\mathbf{x}) t^i(0) = (N-1) \mathbf{x}^{-4} (1 + \lambda_{\text{ttD}} \mathbf{x}^3 \text{D}(0) + \dots) \quad (\text{S.9})$$

so for $x \ll L$, we expect

$$\langle t^i(\mathbf{x}) t^i(0) \rangle \approx (N-1) \mathbf{x}^{-4} \left[1 + \lambda_{\text{ttD}} u_{\text{D}} \left(\frac{\mathbf{x}}{L} \right)^3 \right]. \quad (\text{S.10})$$

What are the effects of the displacement perturbation on the above correlator? We may regularize this perturbation as $\delta S = z_0 \int d^2 \mathbf{x} (T^{zz}(\mathbf{x}, z = \epsilon) + T^{zz}(\mathbf{x}, z = L - \epsilon))$ with $\epsilon \rightarrow 0^+$. Then in computing $\langle t^i(\mathbf{x}) t^i(0) \rangle$ we may freely slide one of the T^{zz} insertions to the other boundary so that $\delta S \rightarrow 2z_0 \int d^2 \mathbf{x} T^{zz}(z = L, \mathbf{x})$. Now using the OPE (S.9) the only change to (S.10) is a $1/L$ correction to the second term in brackets coming from a $1/L$ correction to $\langle D \rangle$. We ignore this correction below. Collecting other sources of corrections to scaling:

$$\langle \varphi_{\text{lat}}^i(\mathbf{x}) \varphi_{\text{lat}}^i(0) \rangle = \mathcal{N}_\varphi \mathbf{x}^{-4} \left[1 + B_{\varphi D} \left(\frac{\mathbf{x}}{L} \right)^3 + C \mathbf{x}^{-2} \right]. \quad (\text{S.11})$$

Finally, we discuss the bulk-boundary correlation function $\langle \varphi_{\text{lat}}^i(0, z) \varphi_{\text{lat}}^i(0) \rangle$. With one factor of $t^i(0)$ already on the boundary, we may further fuse $\varphi^i(0, z)$ onto the boundary to get for $z \rightarrow 0$

$$\varphi^i(0, z) t^i(0) = 2^{2-\Delta_\varphi} (N-1) b_t z^{-2-\Delta_\varphi} (1 + \beta z^3 \text{D}(0) + \dots). \quad (\text{S.12})$$

The constant in front is fixed by taking the expectation value in a semi-infinite geometry and using Eq. (6). We do not expect the constant β to be related to any of the OPE coefficients already introduced. Taking the expectation value,

$$\begin{aligned} \langle \varphi^i(0, z) t^i(0) \rangle \\ \approx 2^{2-\Delta_\varphi} (N-1) b_t z^{-2-\Delta_\varphi} \left[1 + \beta u_{\text{D}} \left(\frac{z}{L} \right)^3 \right]. \end{aligned} \quad (\text{S.13})$$

By a familiar argument, including corrections from the boundary displacement perturbation results in $z \rightarrow z + z_0$ in the above expression up to a $1/L$ correction to the second term in the brackets. Finally, including other sources of corrections to scaling we obtain Eq. (13) with

$$M_\varphi = \sqrt{\mathcal{N}_\varphi \mathcal{N}_{\text{bulk}} (N-1) / N} 2^{2-\Delta_\varphi} b_t. \quad (\text{S.14})$$

THE NORMAL UNIVERSALITY CLASS IN THE ISING MODEL

In this section, we use the results of Refs. [51, 58] to extract the values of universal amplitudes a_σ , b_{D} for the normal universality class of the 3d Ising model.

We begin with a_σ . Using the notation of Ref. [51],

$$\langle \sigma_{\text{lat}}(z) \rangle = B_M c_\pm (z / \xi_{\pm,0,\text{gap}})^{-\Delta_\sigma}, \quad z \rightarrow 0. \quad (\text{S.15})$$

The non-universal constant B_M is defined so that in the ordered phase in infinite volume

$$\langle \sigma_{\text{lat}} \rangle = B_M (-t)^{\Delta_\sigma \nu} \quad (\text{S.16})$$

with $t = (T - T_c) / T_c$ and ν — the correlation length exponent. The non-universal numbers $\xi_{\pm,0,\text{gap}}$ are defined via

$$\xi_{\pm,\text{gap}} = \xi_{\pm,0,\text{gap}} |t|^{-\nu}, \quad (\text{S.17})$$

where $\xi_{\pm,\text{gap}}$ is the correlation length governing exponential decay of σ correlation function at large distance in the high and low temperature phases. The constants c_\pm in Eq. (S.15) are universal. Now, let $\sigma(x)$ be a continuum field normalized in the bulk at the critical point to $\langle \sigma(x) \sigma(0) \rangle = x^{-2\Delta_\sigma}$. We have in the ordered phase in the bulk

$$\langle \sigma \rangle = u \xi_{-,\text{gap}}^{-\Delta_\sigma}, \quad (\text{S.18})$$

where u is a universal constant that we will be able to relate to other known universal constants below. Now, with $\sigma_{\text{lat}} = \sqrt{N_b} \sigma$, combining (S.16), (S.18), (S.17), we have

$$B_M = \sqrt{N_b} u \xi_{-,\text{gap}}^{-\Delta_\sigma}. \quad (\text{S.19})$$

At the critical point for the normal class,

$$\langle \sigma(z) \rangle = \frac{a_\sigma}{(2z)^{\Delta_\sigma}}. \quad (\text{S.20})$$

Matching this to (S.15) and using (S.19),

$$a_\sigma = 2^{\Delta_\sigma} u c_-. \quad (\text{S.21})$$

Now, from (S.15), $c_+ / c_- = U_{\xi,\text{gap}}^{-\Delta_\sigma}$, where the universal constant $U_{\xi,\text{gap}} = \frac{\xi_{+,0,\text{gap}}}{\xi_{-,0,\text{gap}}}$,

$$a_\sigma = (2U_{\xi,\text{gap}})^{\Delta_\sigma} u c_+. \quad (\text{S.22})$$

We next relate u to known universal constants. Unless otherwise stated, we use the notation of Ref. [45]. In the high-temperature phase,

$$\begin{aligned} G_{\text{lat}}(q) = \int d^d x e^{-i\vec{q}\cdot\vec{x}} \langle \sigma_{\text{lat}}(x) \sigma_{\text{lat}}(0) \rangle \\ \stackrel{q\xi_{+,2} \gg 1}{\approx} \frac{G_{\text{lat}}(q=0) A_1^+}{(q\xi_{+,2})^{d-2\Delta_\sigma}}, \end{aligned} \quad (\text{S.23})$$

where $\xi_{+,2}$ is the second moment correlation length and A_1^+ is a universal number. Further,

$$G_{\text{lat}}(q=0) = C^+ t^{-\nu(d-2\Delta_\sigma)} = C^+ (\xi_{+, \text{gap}}/\xi_{+,0, \text{gap}})^{d-2\Delta_\sigma}. \quad (\text{S.24})$$

with C^+ – a non-universal coefficient. Thus,

$$G_{\text{lat}}(q) = C^+ A_1^+ \left(\frac{\xi_{+, \text{gap}}}{\xi_{+,0, \text{gap}}} \frac{1}{q\xi_{+,2}} \right)^{d-2\Delta_\sigma}, \quad q\xi_{+,2} \gg 1. \quad (\text{S.25})$$

Matching to the bulk normalization of the two-point function of the continuum field $\sigma(x)$, we obtain

$$N_b = \frac{C^+ A_1^+ \Gamma(\Delta_\sigma)}{\pi^{d/2} \Gamma(d/2 - \Delta_\sigma)} \left(\frac{\xi_{+, \text{gap}}}{2\xi_{+,2}\xi_{+,0, \text{gap}}} \right)^{d-2\Delta_\sigma}. \quad (\text{S.26})$$

Then from Eq. (S.19),

$$u = \pi^{d/4} 2^{d/2 - \Delta_\sigma} \left(\frac{\Gamma(d/2 - \Delta_\sigma) Q_c}{\Gamma(\Delta_\sigma) A_1^+} \right)^{1/2} \left(\frac{Q_\xi^-}{U_\xi} \right)^{\Delta_\sigma} \quad (\text{S.27})$$

with

$$Q_c = \frac{B_M^2 \xi_{+,0,2}^d}{C^+}, \quad U_\xi = \frac{\xi_{+,0,2}}{\xi_{-,0,2}}, \quad Q_\xi^- = \frac{\xi_{-,0, \text{gap}}}{\xi_{-,0,2}} \quad (\text{S.28})$$

where

$$\xi_{\pm,2} = \xi_{\pm,0,2} |t|^{-\nu}. \quad (\text{S.29})$$

Combining this with (S.22),

$$a_\sigma = (4\pi)^{d/4} \left(\frac{\Gamma(d/2 - \Delta_\sigma) Q_c}{\Gamma(\Delta_\sigma) A_1^+} \right)^{1/2} (Q_\xi^+)^{\Delta_\sigma} c_+ \quad (\text{S.30})$$

with

$$Q_\xi^+ = \frac{\xi_{+,0, \text{gap}}}{\xi_{+,0,2}}. \quad (\text{S.31})$$

Ref. [51] reports $c_+ = 0.844(6)$. We use $\Delta_\sigma = 0.5181489(10)$ [77], $Q_c = 0.3293(2)$ [78], $Q_\xi^+ = 1.000200(3)$ [79]. The greatest uncertainty is on the value of A_1^+ . The value obtained by the ϵ -expansion at 3-loops is $A_1^+ = 0.922$ [80]. This appears consistent with experimental results $A_1^+ = 0.96(4)$, $A_1^+ = 0.95(4)$ [81] (two different parameterizations were used), $A_1^+ = 0.91 - 0.94$ [82], $A_1^+ = 0.915(21)$ [83], as well as roughly consistent with Monte Carlo [84]. We will use the value $A_1^+ \approx 0.915(21)$ from the experimental paper [83]. The value of A_1^+ has the greatest uncertainty out of all the ingredients in the calculation. Combining everything together, we obtain

$$a_\sigma = 2.60(5). \quad (\text{S.32})$$

The truncated bootstrap result is $a_\sigma = 2.5994(8)$ [85], which is spot on.

We next consider the OPE coefficient b_D :

$$T_{zz}(x, z) \sim -\sqrt{C_D} D(x) + \dots, \\ \sigma(x, z) \sim \frac{a_\sigma}{(2z)^{\Delta_\sigma}} + b_D (2z)^{d-\Delta_\sigma} D(x) + \dots. \quad (\text{S.33})$$

Here and below $T^{\mu\nu} = -\frac{2}{\sqrt{g}} \frac{\delta S}{\delta g_{\mu\nu}}$ is the standard stress-energy tensor. As shown by Cardy [67],

$$\frac{b_D}{\Delta_\sigma a_\sigma} = \frac{1}{S_d \sqrt{C_D}} \quad (\text{S.34})$$

with $S_d = \frac{2\pi^{d/2}}{\Gamma(d/2)}$. (Note that our normalization and sign conventions are different from those in Ref. [67]).

Taking the expectation value in a film geometry of thickness L , we have

$$\langle T_{zz}(z) \rangle = -\sqrt{C_D} \langle D \rangle, \\ \langle \sigma(z) \rangle = \frac{a_\sigma}{(2z)^{\Delta_\sigma}} \left(1 + \frac{b_D}{a_\sigma} (2z)^d \langle D \rangle + \dots \right) \\ = \frac{a_\sigma}{(2z)^{\Delta_\sigma}} \left(1 + B_\sigma \left(\frac{z}{L} \right)^d + \dots \right) \quad (\text{S.35})$$

with

$$B_\sigma = \frac{\Delta_\sigma}{S_d \sqrt{C_D}} (2L)^d \langle D \rangle. \quad (\text{S.36})$$

Finally, with the free energy $F = -\log Z$, where Z is the partition function, let the universal contribution to the free energy of the film per unit surface area, F/L_{\parallel}^{d-1} , be

$$f = \frac{A}{L^{d-1}} \quad (\text{S.37})$$

with A - a universal coefficient. Then

$$\frac{df}{dL} = -\langle T_{zz} \rangle, \quad (\text{S.38})$$

i.e.

$$A = -\frac{\sqrt{C_D} \langle D \rangle L^d}{d-1}, \quad (\text{S.39})$$

so

$$\frac{B_\sigma}{A} = -\frac{2^d (d-1) \Delta_\sigma}{S_d C_D}. \quad (\text{S.40})$$

Now, for ++ boundary conditions on the two surfaces of the slab, Ref. [51] gives $B_\sigma = 1.40(1)$, while Ref. [58] gives $(d-1)A = -0.820(15)$, so

$$C_D = 0.193(5), \quad b_D = 0.244(8). \quad (\text{S.41})$$

In comparison, truncated bootstrap gives $b_D = 0.25064(6)$. Thus, MC and truncated bootstrap values of b_D agree within error-bars.

FITS OF STATISTICALLY CORRELATED DATA

In this work we determine the amplitudes of various one- and two-point functions by fitting the space and size dependence of the MC results. The determination of the best fit parameters is done with the χ^2 minimization. In every fit, all points at a given lattice size originate from the same MC run, hence they are statistically correlated. Taking such a correlation into account is essential in order to reliably estimate the uncertainty of the fitted parameters. In principle, the fit procedure can be naturally adapted to take a statistical covariance of data into account, by employing the inverse of the covariance matrix in the formula for χ^2 . Although resampling methods like the Jackknife [71] used here allow to estimate the covariance matrix, it is well known that its inversion is numerically unstable, and can lead to wrong results in the final estimates [72, 73]. Therefore, as we did in Ref. [51], to correctly estimate the uncertainty of the fit parameters, we resort to using the Jackknife resampling method in the computation of the χ^2 itself. Specifically, given a set of MC estimates $\{O_i\}$, we consider the Jackknife bin estimate $\{O_i^J\}$, calculated using all MC data except the discarded MC bin J . Given a fit to a function $f(\{O_i\}, \{p_i\})$, depending on parameters $\{p_i\}$ that we want to determine, we minimize

$$(\chi^2)^J = \sum_i \left(\frac{O_i^J - f(\{O_i^J\}, \{p_i\})}{\sigma_i^2} \right)^2, \quad (\text{S.42})$$

where σ_i is an estimate of the uncertainty of O_i , computed with the usual Jackknife [71]. For $J = 1 \dots N_{\text{bin}}$, the minimization of Eq. (S.42) delivers N_{bin} Jackknife estimates of $\{p_i^J\}$, from which the uncertainty is computed with the usual Jackknife formula. In the analysis done below, we have chosen $N_{\text{bin}} = 100$. We have further employed the fitted values $\{p_i\}$ obtained using the mean-value estimates of $\{O_i\}$ to subtract the Jackknife bias $\propto 1/N_{\text{bin}}$ in the estimates of $\{p_i\}$; as expected, such a correction is negligible with respect to the statistical error bar. We have also used the dispersion over the Jackknife bins of the minimum $(\chi^2)^J$ to estimate the standard deviation of the minimum χ^2 .

FITS OF ONE- AND TWO-POINT FUNCTIONS

$$N = 2$$

Bulk correlations

As mentioned in the main text, we simulated the ϕ^4 model with periodic BCs at the critical point, for lattice sizes $L = 32 - 192$. The rescaled two-point function shown in Fig. 1(a) suggests that the universal part of the correlations is found for $x \gtrsim 4$. In Tables S.I and S.II, we show results of fits to Eq. (7), as a function of a minimum value x_{min} of x , the maximum value $(x/L)_{\text{max}}$ of x/L and the minimum lattice size L

taken into account. In order to evaluate the possible systematic error due to the uncertainty in the critical exponents Δ_ϕ and Δ_ϵ , in the fits we vary the value of $\Delta_\phi = 0.519088(22)$ and $\Delta_\epsilon = 1.51136(22)$ [70] within one error bar. The quoted error is the sum (in absolute value) of the statistical error bar stemming from the minimization of the $\chi^2/\text{d.o.f.}$ (d.o.f. denotes the degrees of freedom), and the variation of the fitted value due to the uncertainty in Δ_ϕ and Δ_ϵ . Within the high accuracy of our MC data, the last contribution is not completely negligible, but it is typically smaller, or of the same order, as the statistical error bars. Fits for $x_{\text{min}} = 4$ (Table S.I) exhibit a large $\chi^2/\text{d.o.f.}$, which does not improve when $(x/L)_{\text{max}}$ is decreased to $1/8$. The $\chi^2/\text{d.o.f.}$ is significantly improved when $x_{\text{min}} = 6$ (Table S.II), but still somewhat large for $(x/L)_{\text{max}} = 1/4$. A good $\chi^2/\text{d.o.f.}$ is eventually found for $x_{\text{min}} = 6$ and $(x/L)_{\text{max}} = 1/8$. In this case the results are also very stable on increasing L_{min} and allow us to determine the estimates in Eq. (8).

Surface correlations

As discussed in the main text, in order to implement the normal UC, we simulated the ϕ^4 model at the critical point with open BCs and a symmetry-breaking surface field $h_s = 1.5\beta_s$ for lattice sizes $L = 32 - 192$. In Fig. 2(a) we show the two-point function of the field component φ along the surface, rescaled to the expected large-distance decay exponent 4. We observe a quick increase of the error bars on increasing the distance \mathbf{x} . This is due to the relatively fast decay \mathbf{x}^{-4} of the correlations, which requires an increasing computational effort to estimate the amplitude of the correlations $\langle \varphi(\mathbf{x})\varphi(0) \rangle \mathbf{x}^4$. In consideration of the fact that the size dependence in Fig. 2(a) appears to be rather small, we have fitted the MC data to Eq. (9), where finite-size corrections are neglected. Fig. 2(a) suggests that the universal part of the cor-

$(x/L)_{\text{max}}$	L_{min}	N_{bulk}	B_ϵ	C	$\chi^2/\text{d.o.f.}$
1/4	32	0.281034(69)	2.8017(39)	0.3457(30)	10.3(2.3)
	48	0.281004(68)	2.8055(44)	0.3478(29)	9.7(2.4)
	64	0.280957(64)	2.8126(50)	0.3513(27)	7.6(2.3)
	96	0.280922(57)	2.8206(63)	0.3541(23)	5.4(2.0)
	128	0.280954(54)	2.8190(75)	0.3532(21)	5.2(2.4)
1/8	32	0.281180(75)	2.7702(58)	0.3404(31)	12.8(2.6)
	48	0.281164(76)	2.7728(64)	0.3412(32)	12.9(2.7)
	64	0.281090(76)	2.7870(76)	0.3452(32)	11.8(3.0)
	96	0.280991(72)	2.8081(93)	0.3506(30)	9.6(3.0)
	128	0.280960(66)	2.819(10)	0.3527(27)	9.5(3.4)

TABLE S.I. Fits of the bulk two-point function for $N = 2$ to Eq. (7) as a function of the minimum lattice size L_{min} , and of the maximum value of (x/L) taken into account. For all fits we consider MC data for $x \geq x_{\text{min}} = 4$. The quoted error bars are the sum of the statistical uncertainty originating from the fit, and the dependence of the results on varying $\Delta_\phi = 0.519088(22)$, $\Delta_\epsilon = 1.51136(22)$ [70] within one error bar.

$(x/L)_{\max}$	L_{\min}	$\mathcal{N}_{\text{bulk}}$	B_{ϵ}	C	$\chi^2/\text{d.o.f.}$
1/4	32	0.28132(11)	2.7936(44)	0.291(11)	4.4(1.4)
	48	0.28131(11)	2.7941(49)	0.292(12)	4.4(1.4)
	64	0.28126(11)	2.7984(56)	0.301(11)	3.8(1.6)
	96	0.281181(99)	2.8060(67)	0.3132(98)	2.8(1.5)
1/8	128	0.281216(89)	2.8025(75)	0.3119(86)	2.6(1.9)
	48	0.28155(12)	2.7567(82)	0.277(11)	1.12(99)
	64	0.28154(13)	2.7580(99)	0.278(12)	1.1(1.0)
	96	0.28148(14)	2.765(13)	0.284(13)	1.0(1.2)
	128	0.28151(14)	2.761(15)	0.281(14)	1.2(1.4)

TABLE S.II. Same as Table S.I for $x_{\min} = 6$.

$(\mathbf{x}/L)_{\max}$	L_{\min}	\mathcal{N}_{φ}	C	$\chi^2/\text{d.o.f.}$
1/8	32	0.33938(42)	0.192(20)	4.72(66)
	48	0.33935(42)	0.194(20)	4.74(68)
	64	0.33924(43)	0.199(20)	4.94(72)
	96	0.33906(47)	0.207(22)	5.02(74)
1/12	128	0.33929(56)	0.196(26)	5.02(77)
	48	0.33950(45)	0.187(21)	7.7(1.2)
	64	0.33951(45)	0.186(21)	8.0(1.2)
	96	0.33917(47)	0.202(23)	8.0(1.2)
	128	0.33937(55)	0.192(26)	8.0(1.3)

TABLE S.III. Fits of the surface two-point function for $N = 2$ to Eq. (9) as a function of the minimum lattice size L_{\min} , and of the maximum value of (\mathbf{x}/L) taken into account. For all fits we consider MC data for $\mathbf{x} \geq \mathbf{x}_{\min} = 4$.

relations is found for $\mathbf{x} \gtrsim 4$. In Tables S.III and S.IV we report fit results, as a function of a minimum value \mathbf{x}_{\min} of \mathbf{x} , the maximum value $(\mathbf{x}/L)_{\max}$ of \mathbf{x}/L and the minimum lattice size L_{\min} taken into account. Due to the aforementioned rapid increase of statistical error bars, compared to the fits to Eq. (7) we consider in this case smaller values of $(\mathbf{x}/L)_{\max}$. Fits for $\mathbf{x}_{\min} = 4$ reported in Table S.III exhibit a large value of $\chi^2/\text{d.o.f.}$. A good value of $\chi^2/\text{d.o.f.}$ is instead found for $\mathbf{x}_{\min} = 6$ (Table S.IV), and the corresponding fitted values are stable on decreasing $(\mathbf{x}/L)_{\max}$ and increasing L_{\min} . Accordingly, a conservative estimate of \mathcal{N}_{φ} , compatible with all results of Table S.IV is given in Eq. (10).

$(\mathbf{x}/L)_{\max}$	L_{\min}	$\mathcal{N}_{\text{bulk}}$	C	$\chi^2/\text{d.o.f.}$
1/8	48	0.3284(19)	1.20(22)	0.82(32)
	64	0.3285(19)	1.17(22)	0.80(32)
	96	0.3282(19)	1.20(22)	0.83(32)
	128	0.3269(21)	1.38(26)	0.80(34)
1/12	96	0.3278(19)	1.25(23)	0.74(43)
	128	0.3272(21)	1.36(26)	0.77(45)

TABLE S.IV. Same as Table S.III for $\mathbf{x}_{\min} = 6$.

Magnetization profile

The magnetization profile $\langle \sigma(z) \rangle$ shown in Fig. 2(c), for a surface field $h_s = 1.5\beta_s$, and lattice sizes $L = 32 - 192$, displays clearly scaling corrections and finite-size effects. In line with the discussion of the scaling forms, we have fitted the MC to Eq. (11), where we take into account the leading scaling correction $\propto z^{-1}$ and the leading finite-size term. In Tables S.V-S.VII we report results of fits to Eq. (11), as a function of a minimum value z_{\min} of z , the maximum value $(z/L)_{\max}$ of z/L and the minimum lattice size L_{\min} taken into account. The impact of varying $\Delta_{\phi} = 0.519088(22)$ [70] within one error bar mainly affects the precision of M_{σ} . Fits for $z_{\min} = 4$ (Table S.V) exhibit a large $\chi^2/\text{d.o.f.}$, which for $z_{\min} = 6$ (Table S.VI) is substantially reduced, and is compatible with 1 within one estimated standard deviation. As a further check, in Table S.VII we consider fits for $z_{\min} = 8$: in this case we have $\chi^2/\text{d.o.f.} < 1$ for $L_{\min} \geq 64$. The fit results differ only slightly from those of Table S.VI. Judging conservatively the variation in the fit results, we arrive to the estimates of Eq. (12).

Surface-bulk correlations

The rescaled surface-bulk correlation function $\langle \varphi(0)\varphi(0, z) \rangle$ shown in Fig. 2(e) clearly displays scaling corrections, as well as a finite-size dependence. Compared to the order-parameter profile, Fig. 2(c), in Fig. 2(e) scaling corrections appear optically larger, whereas finite-size corrections are smaller. We have attempted to fit the surface-bulk correlation to

$$\langle \varphi(0)\varphi(0, z) \rangle = M_{\varphi}(z + z_0)^{-2-\Delta_{\phi}} \left[1 + B_{\varphi} \left(\frac{z + z_0}{L} \right)^3 \right], \quad (\text{S.43})$$

where we have included the leading corrections only. Fits to Eq. (S.43) (not reported here) give rather unstable results and a large value of $\chi^2/\text{d.o.f.}$. In particular, we observe a rather poor determination of the finite-size correction B_{φ} , and a fitted value of z_0 which deviates from the result of Eq. (12). On increasing the value of z_{\min} the fitted value of z_0 slowly increases, though remaining incompatible with Eq. (12). At the same time, the minimum $\chi^2/\text{d.o.f.}$ reduces, although it remains somewhat large $\chi^2/\text{d.o.f.} \sim 1.5$ for $z_{\min} = 8$. In line with the observations above on Fig. 2(e), we interpret these observations as a sign that subleading scaling corrections are numerically relevant, and that the finite-size term is small. Guided by these consideration, we fit the MC data to Eq. (13) using the result for z_0 given in Eq. (12), and varying its value within one error bar quoted there. Here, the uncertainty of $\Delta_{\phi} = 0.519088(22)$ [70] gives a negligible contribution to the error bars of the fitted parameters.

In Tables S.VIII-S.X we report results of fits to Eq. (13). Analogous to the previous sections, we consider in the fits MC data for $z \geq z_{\min}$, $(z/L) \leq (z/L)_{\max}$, and $L \geq L_{\min}$.

$(z/L)_{\max}$	L_{\min}	M_{σ}	B_{σ}	z_0	$\chi^2/\text{d.o.f.}$
1/4	32	0.754574(93)	1.2150(42)	1.03263(92)	9.0(1.5)
	48	0.754534(94)	1.2258(57)	1.03196(93)	8.3(1.4)
	64	0.754514(94)	1.2304(73)	1.03156(93)	8.5(1.5)
	96	0.754513(93)	1.2240(89)	1.03145(91)	8.8(1.6)
	128	0.754528(96)	1.203(11)	1.03157(94)	8.9(1.6)
1/8	32	0.754685(91)	1.126(15)	1.03394(86)	11.6(2.2)
	48	0.754680(95)	1.130(19)	1.03388(91)	11.8(2.2)
	64	0.754689(98)	1.115(25)	1.03397(96)	12.0(2.3)
	96	0.75477(10)	1.012(37)	1.0351(10)	10.3(2.7)
	128	0.754807(99)	0.925(43)	1.03557(98)	10.2(2.8)

TABLE S.V. Fits of the order-parameter profile for $N = 2$ to Eq. (11) as a function of the minimum lattice size L_{\min} , and of the maximum value of (z/L) taken into account. For all fits we consider MC data for $z \geq z_{\min} = 4$. The quoted error bars are the sum of the statistical uncertainty originating from the fit, and the dependence of the results on varying $\Delta_{\phi} = 0.519088(22)$ [70] within one error bar.

$(z/L)_{\max}$	L_{\min}	M_{σ}	B_{σ}	z_0	$\chi^2/\text{d.o.f.}$
1/4	32	0.75428(12)	1.2319(44)	1.0251(17)	4.29(88)
	48	0.75419(12)	1.2478(61)	1.0232(18)	2.68(72)
	64	0.75412(13)	1.2613(79)	1.0216(18)	1.71(58)
	96	0.75410(12)	1.2630(95)	1.0211(18)	1.75(62)
	128	0.75412(12)	1.249(12)	1.0212(17)	1.31(55)
1/8	48	0.75430(12)	1.171(20)	1.0247(17)	1.73(80)
	64	0.75427(13)	1.185(27)	1.0243(18)	1.66(76)
	96	0.75430(15)	1.161(45)	1.0248(22)	1.55(88)
	128	0.75431(15)	1.139(54)	1.0247(22)	1.4(1.0)

TABLE S.VI. Same as Table S.V for $z_{\min} = 6$.

We first consider fits where the finite-size correction is ignored, i.e., we fix $B_{\varphi} = 0$ in Eq. (13). Fits for $z_{\min} = 4$ (Table S.VIII) exhibit a large value of $\chi^2/\text{d.o.f.}$. The quality of the fits is substantially improved when we restrict the data to $z_{\min} = 6$ (Table S.IX), although the value of $\chi^2/\text{d.o.f.}$ is still somewhat large. The inclusion of the finite-size term $B_{\varphi}(z/L)^3$ in the fits further improves the fits, giving a good $\chi^2/\text{d.o.f.}$. In agreement with the observations above, the fitted value of B_{φ} is small, and appears to be difficult to resolve with precision. The fitted amplitude M_{φ} is instead very stable and precise. As an additional check of the robustness of the results, in Table S.X we repeat the fits for $z_{\min} = 8$, obtaining results in line with those found for $z_{\min} = 6$. By considering the variation of the fit results in Tables S.IX and S.X, we extract the estimates of Eq. (14).

$$N = 3$$

Bulk correlations

We proceed here analogous to the XY case. The rescaled bulk two-point shown in Fig. 1(b) suggests that its universal part is found for $x \gtrsim 4$. In Tables S.XI-S.XIII we show fits to the Eq. (7), where we also consider the variation of $\Delta_{\phi} = 0.518920(25)$ and $\Delta_{\epsilon} = 1.5948(2)$ [56] within one error bar. Fits for $x_{\min} = 4$ (Table S.XI) display a large

$\chi^2/\text{d.o.f.}$. For $x_{\min} = 6$ (Table S.XII) we observe a significant decrease of $\chi^2/\text{d.o.f.}$, which becomes compatible with 1 within one standard deviation for $(x/L)_{\max} = 1/8$; further decreasing $(x/L)_{\max}$ does not alter the minimum $\chi^2/\text{d.o.f.}$. As a further check, we considered $x_{\min} = 8$. Corresponding fit results shown in Table S.XIII exhibits a small $\chi^2/\text{d.o.f.}$ for $(x/L)_{\max} = 1/8$ and the fitted values of $\mathcal{N}_{\text{bulk}}$ are in agreement with the results for $x_{\min} = 6$ and $(x/L)_{\max} = 1/8$. Based on these fits, we arrive to the estimates of Eq. (15).

Surface correlations

We observe in the surface correlations of the field component φ shown in Fig. 2(b) a rapid increase of the error bars on increasing the distance \mathbf{x} . Similar to the $N = 2$ case (Fig. 2(a)), this is due to the fast decay of correlations.

In Tables S.XIV and S.XV we report results of fits to Eq. (9), as a function of L_{\min} , $(\mathbf{x}/L)_{\max}$, and for two values of the minimum separation \mathbf{x}_{\min} considered. Fits for $\mathbf{x}_{\min} = 4$ (Table S.XIV) exhibit a large value of $\chi^2/\text{d.o.f.}$. Increasing \mathbf{x}_{\min} to $\mathbf{x}_{\min} = 6$ (Table S.XV) significantly improves the value of $\chi^2/\text{d.o.f.}$. Although in the fits of Table S.XV the central value of $\chi^2/\text{d.o.f.}$ remains somewhat large, we notice that it is nevertheless compatible with 1 within one estimated standard deviation. The inclusion of a finite-size correction $\propto (\mathbf{x}/L)^3$ in the fit Ansatz of Eq. (9) does

$(z/L)_{\max}$	L_{\min}	M_{σ}	B_{σ}	z_0	$\chi^2/\text{d.o.f.}$
1/4	32	0.75413(15)	1.2464(54)	1.0209(28)	2.75(65)
	48	0.75406(16)	1.2560(66)	1.0191(30)	1.89(58)
	64	0.75394(16)	1.2720(88)	1.0159(31)	0.81(37)
	96	0.75389(16)	1.279(11)	1.0144(32)	0.70(35)
	128	0.75392(16)	1.268(13)	1.0146(31)	0.32(22)
1/8	64	0.75409(17)	1.203(31)	1.0187(31)	0.34(31)
	96	0.75410(20)	1.198(49)	1.0189(38)	0.34(34)
	128	0.75407(22)	1.203(66)	1.0181(43)	0.23(34)

TABLE S.VII. Same as Table S.V for $z_{\min} = 8$.

$(z/L)_{\max}$	L_{\min}	M_{φ}	B_{φ}	C	$\chi^2/\text{d.o.f.}$
1/4	32	0.31163(36)		3.182(72)	11.9(1.2)
	48	0.31169(36)		3.178(72)	10.5(1.2)
	64	0.31177(36)		3.172(73)	10.2(1.2)
	96	0.31188(36)		3.162(72)	10.3(1.3)
	128	0.31196(37)		3.154(74)	11.6(1.5)
1/4	32	0.31186(36)	-0.451(52)	3.162(72)	10.4(1.2)
	48	0.31178(37)	-0.203(91)	3.170(72)	10.4(1.2)
	64	0.31171(37)	0.16(15)	3.177(71)	10.3(1.2)
	96	0.31166(38)	0.93(27)	3.182(72)	9.7(1.2)
	128	0.31172(39)	1.63(42)	3.177(73)	10.7(1.3)
1/8	32	0.31169(36)		3.177(71)	22.5(2.5)
	48	0.31168(36)		3.179(72)	22.5(2.5)
	64	0.31172(36)		3.176(72)	21.9(2.5)
	96	0.31184(36)		3.167(72)	21.7(2.7)
	128	0.31193(37)		3.158(74)	24.3(3.3)
1/8	32	0.31181(37)	-0.58(10)	3.169(71)	21.9(2.5)
	48	0.31181(37)	-0.59(13)	3.169(72)	22.3(2.6)
	64	0.31168(38)	0.19(24)	3.180(72)	22.4(2.6)
	96	0.31133(41)	3.06(52)	3.211(73)	19.2(2.5)
	128	0.31123(43)	6.11(87)	3.219(74)	19.1(2.6)

TABLE S.VIII. Fits of the surface-bulk correlations for $N = 2$ to Eq. (13) as a function of the minimum lattice size L_{\min} , and of the maximum value of (z/L) taken into account. For all fits we use $z_0 = 1.018(6)$ (Eq. (12)) and consider MC data for $z \geq z_{\min} = 4$. The quoted error bars are the sum of the uncertainty stemming from the fit, and the spread of the results on varying z_0 within one error bar quoted in Eq. (12). An absent B_{φ} indicates that we fixed it to $B_{\varphi} = 0$, see main text.

$(z/L)_{\max}$	L_{\min}	M_{φ}	B_{φ}	C	$\chi^2/\text{d.o.f.}$
1/4	32	0.31368(38)		2.78(11)	3.39(48)
	48	0.31369(38)		2.78(11)	2.28(42)
	64	0.31378(38)		2.77(11)	1.67(38)
	96	0.31395(37)		2.75(11)	1.20(30)
	128	0.31421(40)		2.71(11)	1.06(31)
1/4	32	0.31426(38)	-0.615(52)	2.70(11)	1.02(27)
	48	0.31428(38)	-0.638(81)	2.69(10)	1.02(27)
	64	0.31428(39)	-0.63(14)	2.70(10)	1.05(28)
	96	0.31421(42)	-0.47(25)	2.71(11)	1.06(29)
	128	0.31436(43)	-0.39(39)	2.68(11)	1.02(31)
1/8	48	0.31407(38)		2.72(10)	2.12(57)
	64	0.31403(38)		2.73(10)	1.93(58)
	96	0.31406(38)		2.73(10)	1.37(53)
	128	0.31426(40)		2.70(11)	0.96(49)
1/8	48	0.31434(39)	-0.91(15)	2.69(10)	1.11(43)
	64	0.31443(40)	-1.11(23)	2.68(10)	1.07(41)
	96	0.31440(47)	-1.01(53)	2.68(11)	1.14(45)
	128	0.31447(52)	-0.83(87)	2.66(12)	0.92(48)

TABLE S.IX. Same as Table S.VIII for $z_{\min} = 6$.

$(z/L)_{\max}$	L_{\min}	M_{φ}	B_{φ}	C	$\chi^2/\text{d.o.f.}$
1/4	32	0.31378(45)		2.75(18)	2.29(41)
	48	0.31373(44)		2.78(18)	1.96(39)
	64	0.31378(45)		2.79(18)	1.47(36)
	96	0.31394(46)		2.77(18)	1.07(29)
1/4	128	0.31423(50)		2.71(19)	1.00(31)
	32	0.31457(46)	-0.592(64)	2.59(18)	0.84(23)
	48	0.31466(46)	-0.645(84)	2.57(18)	0.82(23)
	64	0.31466(49)	-0.67(14)	2.57(18)	0.84(24)
	96	0.31453(52)	-0.56(24)	2.62(18)	0.90(26)
1/8	128	0.31456(55)	-0.46(38)	2.62(19)	0.96(30)
	64	0.31436(46)		2.63(17)	1.21(48)
	96	0.31428(46)		2.67(17)	0.96(48)
1/8	128	0.31439(49)		2.66(18)	0.77(44)
	64	0.31483(50)	-1.15(30)	2.56(17)	0.59(31)
1/8	96	0.31493(60)	-1.32(57)	2.53(19)	0.60(31)
	128	0.31487(75)	-1.2(1.1)	2.55(23)	0.69(38)

TABLE S.X. Same as Table S.VIII for $z_{\min} = 8$.

$(x/L)_{\max}$	L_{\min}	$\mathcal{N}_{\text{bulk}}$	B_{ϵ}	C	$\chi^2/\text{d.o.f.}$
1/4	32	0.311698(62)	2.4795(33)	0.3484(21)	22.0(3.0)
	48	0.311660(59)	2.4849(37)	0.3507(19)	19.2(2.9)
	64	0.311631(57)	2.4901(41)	0.3527(18)	16.3(2.8)
	96	0.311617(54)	2.4944(50)	0.3539(17)	14.0(2.8)
	128	0.311636(51)	2.4980(63)	0.3537(15)	12.0(2.7)
1/8	32	0.311817(63)	2.4500(43)	0.3443(21)	31.3(4.2)
	48	0.311793(63)	2.4546(48)	0.3454(21)	31.0(4.3)
	64	0.311742(62)	2.4660(55)	0.3480(20)	29.5(4.5)
1/8	96	0.311676(61)	2.4823(67)	0.3512(20)	27.7(4.8)
	128	0.311622(55)	2.5035(82)	0.3542(17)	24.3(4.8)

TABLE S.XI. Fits of the bulk two-point function for $N = 3$ to Eq. (7) as a function of the minimum lattice size L_{\min} , and of the maximum value of (x/L) taken into account. For all fits we consider MC data for $x \geq x_{\min} = 4$. The quoted error bars are the sum of the statistical uncertainty originating from the fit, and the dependence of the results on varying $\Delta_{\phi} = 0.518920(25)$ and $\Delta_{\epsilon} = 1.5948(2)$ [56] within one error bar.

$(x/L)_{\max}$	L_{\min}	$\mathcal{N}_{\text{bulk}}$	B_{ϵ}	C	$\chi^2/\text{d.o.f.}$
1/4	32	0.311987(92)	2.4714(32)	0.3000(73)	7.6(1.3)
	48	0.311974(90)	2.4724(36)	0.3019(71)	7.4(1.4)
	64	0.311941(87)	2.4752(40)	0.3068(68)	6.5(1.5)
	96	0.311917(83)	2.4775(48)	0.3114(64)	5.5(1.6)
	128	0.311921(76)	2.4793(60)	0.3139(56)	4.1(1.7)
1/8	48	0.312214(96)	2.4324(56)	0.2846(70)	1.3(1.0)
	64	0.312207(99)	2.4333(63)	0.2853(74)	1.3(1.0)
	96	0.31220(10)	2.4348(82)	0.2863(80)	1.4(1.2)
128	0.31217(10)	2.439(10)	0.2894(79)	1.5(1.5)	

TABLE S.XII. Same as Table S.XI for $x_{\min} = 6$.

not significantly change the $\chi^2/\text{d.o.f.}$: indeed, Fig. 2(b) suggests a size dependence which is smaller than the statistical error bars. From Table S.XV we obtain the estimates given in Eq. (16).

$(x/L)_{\max}$	L_{\min}	$\mathcal{N}_{\text{bulk}}$	B_{ϵ}	C	$\chi^2/\text{d.o.f.}$
1/4	32	0.31195(13)	2.4770(37)	0.297(18)	5.9(1.2)
	48	0.31197(13)	2.4758(40)	0.293(19)	5.9(1.2)
	64	0.31195(13)	2.4770(45)	0.299(19)	5.6(1.3)
	96	0.31191(12)	2.4788(55)	0.310(19)	5.0(1.5)
	128	0.31188(11)	2.4820(64)	0.325(16)	3.9(1.6)
1/8	64	0.31229(14)	2.4318(79)	0.260(18)	0.42(63)
	96	0.31230(15)	2.4305(97)	0.258(20)	0.41(61)
128	0.31231(17)	2.428(14)	0.256(24)	0.46(70)	

TABLE S.XIII. Same as Table S.XI for $x_{\min} = 8$.

$(\mathbf{x}/L)_{\max}$	L_{\min}	\mathcal{N}_{φ}	C	$\chi^2/\text{d.o.f.}$
1/8	32	0.50134(45)	0.207(15)	11.6(1.0)
	48	0.50132(45)	0.209(15)	11.8(1.0)
	64	0.50112(47)	0.215(15)	12.2(1.1)
	96	0.50076(49)	0.226(16)	12.1(1.1)
	128	0.50024(51)	0.243(17)	12.7(1.3)
1/12	48	0.50161(46)	0.198(15)	19.3(1.7)
	64	0.50161(46)	0.199(15)	20.1(1.8)
	96	0.50091(48)	0.222(16)	20.1(1.9)
128	0.50025(51)	0.242(17)	21.4(2.2)	

TABLE S.XIV. Fits of the surface two-point function for $N = 3$ to Eq. (9) as a function of the minimum lattice size L_{\min} , and of the maximum value of (x/L) taken into account. For all fits we consider MC data for $\mathbf{x} \geq \mathbf{x}_{\min} = 4$.

Magnetization profile

The rescaled order-parameter profile $\langle \sigma(z) \rangle$ shown in Fig. 2(d) exhibits scaling corrections and finite-size effects, similar to the $N = 2$ case.

In Tables S.XVI-S.XVIII we report fit results, as a function of a minimum value z_{\min} of z , the maximum value $(z/L)_{\max}$ of z/L and the minimum lattice size L_{\min} taken into account.

$(\mathbf{x}/L)_{\max}$	L_{\min}	\mathcal{N}_φ	C	$\chi^2/\text{d.o.f.}$
1/8	48	0.4818(21)	1.49(17)	1.47(42)
	64	0.4818(21)	1.49(17)	1.51(43)
	96	0.4821(22)	1.46(18)	1.61(46)
1/12	128	0.4816(23)	1.48(20)	1.64(53)
	96	0.4809(23)	1.56(19)	1.52(59)
	128	0.4805(24)	1.58(21)	1.37(62)

TABLE S.XV. Same as Table S.XIV for $\mathbf{x}_{\min} = 6$.

As in the case $N = 2$, we additionally vary the exponent $\Delta_\phi = 0.518920(25)$ [56] within one error bar, and add the resulting variation to the statistical error bars arising from the fits.

Fits for $z_{\min} = 4$ (Table S.XVI) exhibit a large $\chi^2/\text{d.o.f.}$. Its value is significantly reduced when we increase z_{\min} to $z_{\min} = 6$ (Table S.XVII) and $z_{\min} = 8$ (Table S.XVIII). Nevertheless, we observe also in these cases a large $\chi^2/\text{d.o.f.}$ for $(z/L)_{\max} = 1/4$, suggesting that, within the precision of MC data, the order-parameter profile is not well approximated by Eq. (11), when $(z/L)_{\max} \sim 1/4$. Restricting the fit to $(z/L)_{\max} = 1/8$, we obtain a good $\chi^2/\text{d.o.f.}$ for $z_{\min} = 8$, while for $z_{\min} = 6$ the value of $\chi^2/\text{d.o.f.}$ is nevertheless compatible with 1, within one standard deviation. Irrespective of

the above considerations on the quality of the fit, we notice that the fitted value of M_σ in Tables S.XVII and S.XVIII is extremely stable. Judging conservatively the variation in the results of Tables S.XVII and S.XVIII for $(z/L)_{\max} = 1/8$, we can obtain the estimate given in Eq. (17).

Surface-bulk correlations

Similar to the $N = 2$ case (Fig. 2(e)), in rescaled surface-bulk correlation function $\langle \vec{\varphi}(0) \cdot \vec{\varphi}(0, z) \rangle$ shown in Fig. 2(f) we also observe significant scaling corrections, and comparatively smaller finite-size corrections. A quantitative analysis of the correlations $\langle \vec{\varphi}(0) \cdot \vec{\varphi}(0, z) \rangle$ presents the same challenges as for the $N = 2$ case. In particular, fits to Eq. (S.43) provide unstable results. As in the $N = 2$ case, we fit the MC data to Eq. (13), using the value of z_0 determined in Eq. (17) from the order-parameter profile. In Tables S.XIX-S.XXI we present the fit results. While fits for $z_{\min} = 4$ (Table S.XIX) give a large $\chi^2/\text{d.o.f.}$, restricting the data to $z_{\min} = 6$ (Table S.XX) and $z_{\min} = 8$ (Table S.XXI) gives stable and consistent results especially for the amplitude M_φ , while the amplitude of the finite-size correction B_φ can be determined only with a limited precision. Judging conservatively the variation of the results in Tables S.XX and S.XXI we arrive to the estimates of Eq. (18).

$(z/L)_{\max}$	L_{\min}	M_{σ}	B_{σ}	z_0	$\chi^2/\text{d.o.f.}$
1/4	32	0.706517(95)	1.1503(42)	1.03951(97)	9.3(1.2)
	48	0.706468(95)	1.1640(55)	1.03866(97)	7.7(1.2)
	64	0.706470(94)	1.1604(70)	1.03862(96)	7.9(1.2)
	96	0.706473(92)	1.1559(91)	1.03866(91)	8.6(1.3)
	128	0.706490(96)	1.163(13)	1.03883(97)	8.0(1.5)
1/8	32	0.706625(93)	1.065(13)	1.04086(91)	9.8(1.9)
	48	0.706605(96)	1.083(17)	1.04057(95)	9.7(1.9)
	64	0.70663(10)	1.046(23)	1.0410(10)	9.3(2.1)
	96	0.70673(10)	0.927(34)	1.0424(10)	7.0(2.1)
	128	0.706734(99)	0.903(42)	1.0425(10)	8.2(2.6)

TABLE S.XVI. Fits of the order-parameter profile for $N = 3$ to Eq. (11) as a function of the minimum lattice size L_{\min} , and of the maximum value of (z/L) taken into account. For all fits we consider MC data for $z \geq z_{\min} = 4$. The quoted error bars are the sum of the statistical uncertainty originating from the fit, and the dependence of the results on varying $\Delta_{\phi} = 0.518920(25)$ [56] within one error bar.

$(z/L)_{\max}$	L_{\min}	M_{σ}	B_{σ}	z_0	$\chi^2/\text{d.o.f.}$
1/4	32	0.70626(12)	1.1659(41)	1.0328(18)	5.11(95)
	48	0.70617(13)	1.1826(55)	1.0307(19)	3.15(91)
	64	0.70614(13)	1.1870(72)	1.0300(19)	3.09(95)
	96	0.70612(12)	1.1914(90)	1.0293(18)	3.2(1.1)
	128	0.70612(12)	1.206(13)	1.0289(18)	1.41(51)
1/8	48	0.70630(12)	1.101(18)	1.0326(17)	1.45(94)
	64	0.70631(13)	1.093(24)	1.0328(19)	1.45(98)
	96	0.70637(15)	1.050(42)	1.0341(22)	1.2(1.0)
	128	0.70630(15)	1.107(55)	1.0325(24)	1.09(92)

TABLE S.XVII. Same as Table S.XVI for $z_{\min} = 6$.

$(z/L)_{\max}$	L_{\min}	M_{σ}	B_{σ}	z_0	$\chi^2/\text{d.o.f.}$
1/4	32	0.70617(15)	1.1782(47)	1.0303(30)	3.75(94)
	48	0.70610(16)	1.1872(57)	1.0286(31)	3.00(98)
	64	0.70606(17)	1.1926(79)	1.0273(34)	2.9(1.1)
	96	0.70600(16)	1.2013(97)	1.0253(32)	2.9(1.2)
	128	0.70593(16)	1.225(13)	1.0222(31)	0.50(25)
1/8	64	0.70622(17)	1.091(28)	1.0299(30)	1.00(92)
	96	0.70626(19)	1.072(45)	1.0309(37)	0.95(97)
	128	0.70608(23)	1.171(71)	1.0263(46)	0.17(28)

TABLE S.XVIII. Same as Table S.XVI for $z_{\min} = 8$.

$(z/L)_{\max}$	L_{\min}	M_{φ}	B_{φ}	C	$\chi^2/\text{d.o.f.}$
1/4	32	0.46290(37)		3.318(50)	18.1(1.4)
	48	0.46299(37)		3.314(50)	15.9(1.3)
	64	0.46315(37)		3.305(50)	15.0(1.3)
	96	0.46325(37)		3.299(50)	15.9(1.5)
	128	0.46334(38)		3.294(51)	16.3(1.7)
1/4	32	0.46329(37)	-0.474(42)	3.296(49)	15.4(1.3)
	48	0.46318(38)	-0.284(74)	3.302(49)	15.6(1.3)
	64	0.46307(38)	0.17(11)	3.310(49)	15.1(1.3)
	96	0.46298(39)	0.82(19)	3.315(50)	15.3(1.4)
	128	0.46304(40)	1.34(28)	3.312(50)	15.4(1.5)
1/8	32	0.46301(37)		3.311(49)	33.2(2.8)
	48	0.46300(37)		3.313(49)	33.0(2.8)
	64	0.46308(37)		3.310(49)	31.9(2.9)
	96	0.46318(37)		3.304(50)	33.5(3.2)
	128	0.46329(38)		3.297(51)	34.3(3.5)
1/8	32	0.46319(37)	-0.546(76)	3.304(49)	32.4(2.8)
	48	0.46316(38)	-0.47(11)	3.305(49)	33.0(2.9)
	64	0.46290(38)	0.59(18)	3.319(49)	32.1(3.0)
	96	0.46237(40)	3.51(36)	3.351(49)	28.5(3.0)
	128	0.46225(42)	6.16(58)	3.359(50)	26.1(3.0)

TABLE S.XIX. Fits of the surface-bulk correlations for $N = 3$ to Eq. (13) as a function of the minimum lattice size L_{\min} , and of the maximum value of (z/L) taken into account. For all fits we use $z_0 = 1.031(4)$ (Eq. (17)) and consider MC data for $z \geq z_{\min} = 4$. The quoted error bars are the sum of the uncertainty stemming from the fit, and the spread of the results on varying z_0 within one error bar quoted in Eq. (17). An absent B_{φ} indicates that we fixed it to $B_{\varphi} = 0$, see main text.

$(z/L)_{\max}$	L_{\min}	M_{φ}	B_{φ}	C	$\chi^2/\text{d.o.f.}$
1/4	32	0.46599(39)		2.901(74)	5.73(67)
	48	0.46602(39)		2.906(74)	3.97(56)
	64	0.46622(39)		2.891(73)	2.15(43)
	96	0.46644(39)		2.869(74)	1.67(38)
	128	0.46656(42)		2.858(77)	1.43(41)
1/4	32	0.46692(39)	-0.638(41)	2.813(73)	1.30(27)
	48	0.46704(40)	-0.728(68)	2.800(73)	1.26(27)
	64	0.46693(42)	-0.62(11)	2.814(74)	1.20(28)
	96	0.46693(45)	-0.62(18)	2.814(76)	1.30(31)
	128	0.46686(47)	-0.54(27)	2.824(78)	1.28(38)
1/8	48	0.46664(41)		2.834(74)	2.55(59)
	64	0.46658(41)		2.847(74)	1.88(53)
	96	0.46660(41)		2.848(75)	1.71(52)
	128	0.46664(43)		2.848(77)	1.51(56)
1/8	48	0.46694(42)	-0.70(13)	2.813(74)	1.65(48)
	64	0.46684(44)	-0.53(20)	2.824(76)	1.63(48)
	96	0.46675(51)	-0.30(40)	2.833(81)	1.72(52)
	128	0.46666(55)	-0.06(63)	2.846(83)	1.57(58)

TABLE S.XX. Same as Table S.XIX for $z_{\min} = 6$.

$(z/L)_{\max}$	L_{\min}	M_{φ}	B_{φ}	C	$\chi^2/\text{d.o.f.}$
1/4	32	0.46642(44)	2.80(12)	4.15(59)	
	48	0.46630(44)	2.85(12)	3.38(53)	
	64	0.46640(44)	2.86(12)	2.05(44)	
	96	0.46673(45)	2.81(12)	1.51(39)	
	128	0.46707(51)	2.73(13)	1.26(39)	
1/4	32	0.46763(44)	-0.660(54)	2.65(12)	0.97(23)
	48	0.46782(47)	-0.739(72)	2.62(12)	0.90(22)
	64	0.46774(50)	-0.71(11)	2.64(12)	0.92(23)
	96	0.46793(57)	-0.82(19)	2.60(13)	0.93(24)
	128	0.46802(61)	-0.89(28)	2.56(14)	0.89(29)
1/8	64	0.46739(49)	2.67(12)	0.93(36)	
	96	0.46735(50)	2.68(12)	0.91(35)	
	128	0.46741(53)	2.66(13)	0.84(38)	
1/8	64	0.46761(53)	-0.39(27)	2.64(12)	0.86(32)
	96	0.46762(65)	-0.40(45)	2.64(14)	0.89(33)
	128	0.46797(77)	-0.94(77)	2.57(16)	0.75(32)

TABLE S.XXI. Same as Table S.XIX for $z_{\min} = 8$.